Effect of Buffer on Protein Capture with Weak Cation Exchange Membranes

by

Huayu Niu

A thesis
presented to the University of Waterloo
in fulfillment of the
thesis requirement for the degree of
Master of Applied Science
in
Chemical Engineering

Waterloo, Ontario, Canada, 2015

AUTHOR'S DECLARATION

I hereby declare that I am the sole author of this thesis. This is a true copy of the thesis, including any required final revisions, as accepted by my examiners.

I understand that my thesis may be made electronically available to the public.

_____

Huayu Niu

Abstract

Ion exchange membrane chromatography represents a potential alternative to conventional Protein A or resin chromatography for protein capture of monoclonal antibodies (mAbs), due to its high throughput and low operation cost. Buffer optimization is critical for understanding the performance of ion exchange membrane chromatography.

This project investigates the effect of buffer on membrane properties and protein capture with a weak cation exchange macroporous hydrogel membrane, Natrix C. The weak cation exchange membrane is comprised of a porous polyacrylate hydrogel and a polyolefin matrix backbone, displaying different properties according to buffer conditions. Two types of buffer with different ion characteristics, phosphate citrate buffer (effective pH: 2~8) and acetate buffer (effective pH: 4~5), were evaluated.

In the first part, the effect of buffer on the membrane swelling behavior was investigated, and membrane surface morphology was observed by Environmental Scanning Electron Microscopy (ESEM). Significant influence of pH and ionic strength on membrane swelling was confirmed (ANOVA; 95%) for phosphate citrate and acetate buffer, while no significant difference was observed between the two buffer types. Surface morphology of Natrix C visualized by ESEM indicated the significance of the hydrogel component.

The second part focused on the effect of buffer on static protein adsorption by comparing two model proteins, lysozyme and immunoglobulin G (IgG), through protein adsorption isotherms and adsorption models. The two-parameter Langmuir model indicated different maximum adsorption capacity (q_{max}) and protein membrane affinity (K) according to protein type and buffer conditions. The adsorption isotherm for lysozyme was dominated by the strong protein charge, thus the buffer effect was negligible. As for IgG, the moderate protein charge led to pronounced buffer effect, where the estimated q_{max} and K were significantly different between the two buffers. The difference in the estimated K may result from the effect of ion composition on surface charge distribution of protein, while the estimated q_{max} may reflect the effect of ionic strength on accessibility of binding sites and competitive binding between salt and protein. Protein membrane interactions were studied through the SMA adsorption model on IgG adsorption isotherms, by analyzing the difference of estimated parameters, the characteristic charge (ν), the equilibrium constant (K_a), and the steric factor (σ), between the two buffers. The influence of ion valence was proposed, that multivalent anions in phosphate citrate buffer may adsorb onto the protein surface thus affect its surface charge distribution.

In the last part, the effect of buffer on dynamic protein adsorption, *i.e.* feed protein concentration, pH and type of binding buffer, was analyzed by the breakthrough curves and dynamic binding capacity estimates at 10% breakthrough ($DBC_{10\%}$). Distinct breakthrough curves were observed for lysozyme according to pH, feed concentration and buffer type, indicating different degrees of mass transport limitations. Significant effect of pH and buffer type, and moderate effect of feed concentration on $DBC_{10\%}$ were observed for lysozyme with Natrix C (ANOVA; 95%). Dynamic binding of IgG was strongly dependent on buffer type. Higher $DBC_{10\%}$ than lysozyme was achieved in acetate buffer, while dynamic binding was inoperable with the phosphate citrate buffer.

In general, Natrix C membrane is a promising alternative for protein capture, with its high affinity and high binding capacity as presented in this study. While its performance is significantly influenced by buffer, establishing appropriate procedures for buffer optimization according to protein characteristics is essential for the development of ion exchange membrane chromatography.

Acknowledgements

I would like to express my deepest appreciation to my advisor, Dr. Christine Moresoli, for her guidance and support during my graduate studies at the University of Waterloo. I am grateful for her acceptance of me as her graduate student, giving me the opportunity to conduct research in the field of my interest. She encouraged me to grow as an experimentalist, a researcher, and an independent thinker. Her mentorship has been indispensable in the completion of my thesis, and has been paramount in reaching my career goals.

I would like to acknowledge the Monoclonal Antibody Network (MabNet) of the Natural Sciences and Engineering Research Council of Canada (NSERC) for their financial support. I would also like to thank the Department of Chemical Engineering and the University of Waterloo for their financial support in many ways throughout my graduate studies. I am indebted to Natrix Separations Inc. for generously supplying their membrane material and accessory materials.

My sincere thanks also go to Dr. Marc Aucoin for access to the ÄKTA prime system, and to Nina Heinig and Lei Zhang for their assistance with ESEM.

I would like to express my special appreciation to Dr. Katharina Hassel for her guidance and training on static protein binding, to Rasool Nasseri Pourtakalo for his advices on MATLAB programming, and to other members of the Moresoli research group, Joseph Khouri, Nagma Zerin and Yung Priscilla Lai for their invaluable friendship.

Special thanks to our co-op students, Nils Wagner for his training and technical contributions on the ÄKTA prime system, Robert Ngunjiri for his training on the freeze dryer and to Jason Tran for his continuous support and technical contributions to my research.

I am thankful to the readers of my thesis, Dr. Marc Aucoin and Dr. Bernard Marcos for their time and invaluable feedback.

None of this would have been possible without the love and support from my friends and my family. My encouraging parents, Yuzhu Niu and Xiuli Zhang, gave me a constant source of love and strength all these years.

Finally, my gratitude goes to my significant other Tong Jia, for his inspiration, patience, caring and understanding through good times and bad.

Table of Contents

List of Figures

List of Tables

List of Abbreviations

$\bar{a}_W$	Activities of solvent in solution phase
$\bar{q_s}$ (mmol/L)	Salt concentration in stationary phase
a_W	Activities of solvent in membrane phase
$\bar{d}$	Sample mean of differences
A_0	Absorbance of feed protein solution
ANOVA	Analysis of variance
C_0 (Static binding; mg/mL)	Initial protein concentration
C_a (mmol/L)	Experimental equilibrium protein concentration
C_e (Langmuir; mg/mL)	Equilibrium protein concentration
C_e (SMA; mmol/L)	Equilibrium protein concentration in mobile phase
C_i (mg/mL)	Interfacial solute concentration in liquid phase
CM	Carboxymethyl
C_p (mmol/L)	Protein concentration (non-equilibrium)
C_{po} (DBC; mg/mL)	Initial protein concentration
C_s (Langmuir; dimensionless)	Solute concentration in solid phase
C_s (SMA; mmol/L)	Salt concentration in mobile phase
DBC (mg/mL)	Dynamic binding capacity
$DBC_{10\%}$ (mg/mL)	Dynamic binding capacity at 10% breakthrough
DEAE	Diethylaminoethyl
DMAE	Dimethylaminoethyl
ESEM	Environmental scanning electron microscope
EU	European Union
F_0	Test statistics for ANOVA
FCS	Fluorescence correlation spectroscopy
H_0	Hypothesis
HEW	Hen egg white
IEX	Ion exchange chromatography
Ig	Immunoglobulin
IgG	Immunoglobulin G
K (Langmuir; mL/mg)	Equilibrium constant
k_{-1}	Desorption rate constant
k_1	Adsorption rate constant
K_a (SMA)	Equilibrium constant
K_d (mg/mL)	Dissociation constant
mAbs	Monoclonal antibodies
m_{dry} (g)	Mass of dry membrane
MS	Mean square
$m_{swollen}$ (g)	Mass of wet membrane
MW	Molecular weight
n (Protein adsorption model)	Number of observations
n ′(Langmuir)	Number of transfer units
p	Number of parameters

PCS	Photon correlation spectroscopy
PES	Polyethersulfone
pI	Isoelectric point
PP	Polypropylene
PVDF	Polyvinylidene fluoride
Q	Quaternary ammonium
q (mg/mL)	Adsorbed protein concentration
q’	Saturation capacity
q_a (mg/mL)	Experimental static binding capacity at equilibrium
QAE	Quaternary aminoethyl
q_e (Langmuir; mg/mL)	Adsorbed protein concentration at equilibrium
q_e (SMA; mmol/L)	Adsorbed protein concentration at equilibrium
q_{max} (mg/mL)	Maximum binding capacity
q_{ms}	Swelling factor
q_s (mmol/L)	Salt concentration in stationary phase after protein adsorption
r	Separation factor
R (L atm/K mol)	Gas constant
R^2	Coefficient of determination
R^2_{adj}	Adjusted coefficient of determination
R_A	Reaction rate by adsorption
RC	Regenerated cellulose
R_g	Radius of gyration
R_h	Hydrodynamic radius
S	Sulfo
SANS	Small angle neutron scattering
SAXS	Small angle X-ray scattering
S_d	Sample standard deviation of differences
SDM	Stoichiometric displacement model
SMA	Steric mass-action model
SNAP	Semisynthetic network alginate polymer
SP	Sulfopropyl
SS_A	Sum of squares of factor A
SS_{AB}	Sum of squares of interactions between factor A, B
SS_B	Sum of squares of factor B
SS_E	Sum of squares of error
SS_R	Sum of squares of regression
SS_T	Total sum of squares
T (K)	Thermodynamic temperature
t (s)	Time
t_0	Test statistics for paired t-test
$t_{\alpha/2, n-1}$	Upper $\alpha/2$ percentage point of the t distribution with n-1 degrees of freedom
$V_{membrane}$ (mL)	Total volume of membrane
$V_{permeate}$ (mL)	Total volume of permeate
$V_{solution}$ (mL)	Total volume of binding buffer
V_W (m^3/mol)	Molar volume

Λ (mmol/L)	Ion exchange capacity
ν	Characteristic charge
$\nu 1$	Degree of freedom of A, B, or AB
$\nu 2$	Degree of freedom of error
Π (atm)	Osmotic pressure
σ	Steric factor

Chapter 1
Introduction

1.1 Research Motivation

Over the past few decades, ion exchange has become a leading chromatographic technique employed for the purification of pharmaceutical proteins, especially monoclonal antibodies (mAbs). Ion exchange is used for the purification of mAbs as a polishing step for the removal of impurities. Its use for protein capture has been limited because of lower performance compared to capture by Protein A affinity chromatography [1]. With the recent development of commercial ion exchange membrane materials with high binding, ion exchange membrane chromatography represents a promising alternative to packed-bed chromatography for protein capture, due to its high throughput and low operation cost. A weak cation exchange hydrogel membrane, Natrix C, with a three-dimensional macroporous structure has attracted interest. Containing a high density of carboxylate binding groups, the membrane exhibits high binding capacity [2].

Protein capture with ion exchange chromatography is based on the electrostatic interactions between the oppositely charged protein and membrane, which is dependent on buffer conditions. Therefore, buffer optimization is critical for understanding the performance of ion exchange membrane chromatography.

1.2 Research Objectives

The major objective of the present work was to investigate the effect of buffer on the membrane properties and protein capture with a weak cation exchange macroporous hydrogel membrane, Natrix C. Buffers of interest were phosphate citrate buffer and acetate buffer for their differences in ion valence and ion composition.

The first objective was to investigate the effect of buffer on membrane properties. The effect of pH, ionic strength and buffer type on membrane swelling behavior will be discussed, and membrane surface morphology will be evaluated.

The second objective was to investigate the effect of buffer on protein-membrane interactions during static protein adsorption. Protein adsorption isotherms of two model proteins, lysozyme and IgG, were compared. The parameters of the Langmuir model, maximum adsorption capacity (q_{max}) and equilibrium constant (K), will be estimated to analyze the effect of buffer type and buffer ionic strength for different protein types. For the characterization of protein membrane interactions, analysis of the SMA adsorption

model and IgG adsorption isotherms will be performed for the two buffers. The effect of ion valence and ionic strength will be investigated based on the estimated SMA parameters, characteristic charge (ν), the equilibrium constant (K_a), and the steric factor (σ).

The third objective was to investigate the effect of buffer on dynamic protein adsorption with lysozyme and IgG. The effect of feed protein concentration, pH and type of binding buffer was analyzed by breakthrough curves and dynamic breakthrough at 10% ($DBC_{10\%}$).

Chapter 2
Literature Review

2.1 Ion Exchange Chromatography

Chromatography has become the most effective technique for separating and purifying biomolecules through partitioning and/or adsorption. Proteins can be purified with various chromatography techniques depending on their specific properties, *i.e.* size, hydrophobicity, ligand specificity and surface charge [3]. Separation with affinity chromatography is based on the reversible biological interactions between a specific ligand immobilized on a matrix and the protein. This technique is advantageous for its high selectivity and efficiency, especially in the purification process for monoclonal antibodies (mAbs) [4]. Nevertheless, the cost and the limited lifetime of ligand materials have become bottlenecks in the downstream purification stage of biomolecules [5].

Ion exchange chromatography (IEX) separates proteins according to their distinct charge characteristics. This technique works on the basis of the reversible electrostatic interactions between the charged functional groups on the stationary phase and the protein molecules with opposite charges [6]. With its high resolution and high ligand density, IEX is ideal for capture, for intermediate purification and polishing steps in protein purification and is preferred for the commercial recovery and purification of immunoglobulin G (IgG) from plasma [4].

Depending on the type of stationary phase, IEX can be further divided into packed-bed chromatography and membrane chromatography, as well as cation exchange and anion exchange chromatography.

2.1.1 Packed-bed Chromatography

Packed-bed chromatography is a mature protein purification technique in conventional liquid chromatography. The typical system consists of a glass or steel column packed with porous beads as the ion exchange media (Figure 2-1). The ion exchange matrix is based on inorganic materials, synthetic resins or polysaccharides, generally substituted with specific functional groups that determine its surface charge. The mean particle size of commercial ion exchange resins lies between 3 μm (MiniBeads^{TM}) to 200 μm (Sepharose Big Beads) [3]. The pore size of functionalized, hydrated ion exchange resins is approximately 1 to 2 nm, while macroporous resins have macropores with a size of about 20 to 100 nm [7].

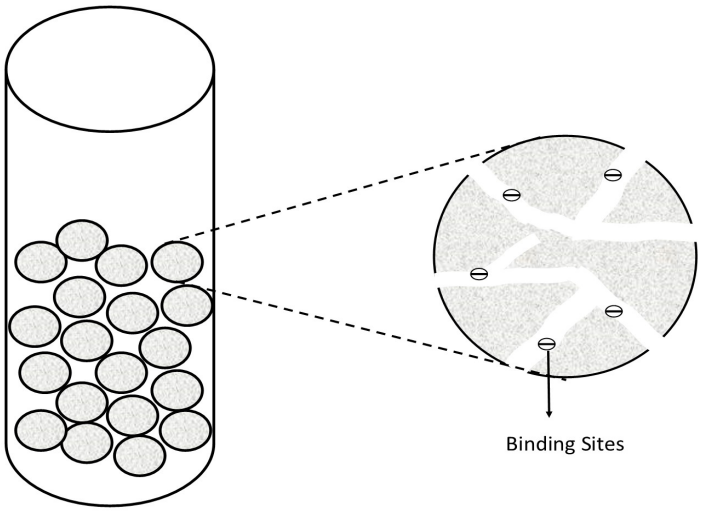

Figure 2-1 Packed-bed chromatography column and porous resin beads.

Properties of the matrix are crucial to the performance of protein purification. An inert matrix with high physical stability and chemical stability eliminates non-specific interactions and ensures reproducibility of the process. The most important property of the matrix is the binding capacity. High capacity results from the high porosity that provides a large surface area with charged groups. For the purification of mAbs, the highest resolution and purity can be achieved with orthogonal principles, where a cation exchange column for intermediate purification and an anion exchange column for impurities removal are applied after the capture step with Protein A [1].

After selection of the matrix and column size for the target protein, operation of a packed-bed chromatography system consists of the following steps [6] :

1. Resin loading in the column; by pouring a slurry of buffer and beads into the column to desired height

2. Sample loading and protein binding; by applying the sample solution with the target protein

3. Target protein elution; by the continuous flow of buffer with desired condition (pH, ionic strength)

4. Collect of the eluent and detection of eluting components

The setup of column chromatography creates several problems. Uneven resin packing may lead to unpredictable fluid distribution and low efficiency. Resin deformation results in high pressure drop across the packed-bed column and also affects productivity [1]. Channeling can also occur when cracks in the resin beads are present and will lead to short-circuiting flow and therefore poor bed utilization [8].

The major drawback with column chromatography lies in the mass transfer limitations that result from porous resin beads [9]. In order to reach the binding sites, the target protein molecules need to travel within the pores of resin beads through intra-particle diffusion. Pore diffusion increases the process time for macromolecules, thus lowers column efficiency and loading capacity. Some of the limitations may be overcome with novel non-porous, rigid chromatographic media [10], or with higher column and lower flow rate; however, the operation cost will increase accordingly [11].

2.1.2 Membrane Chromatography

A promising alternative for packed-bed chromatography is membrane chromatography. By replacing the stationary phase from porous resin beads to thin, microporous or macroporous membranes, mass transport limitations can be significantly reduced (Figure 2-2). In membrane chromatography, the pore size of the membrane is relatively large thus the mass transport of protein molecules to binding sites is dominated by bulk convection. With minimized pore diffusion, higher flow rates are possible to improve productivity. Considerable buffer consumption may also be reduced with shortened overall process time [11]. Compared to column chromatography, membrane chromatography also stands out for its operational and economical advantages. The flow-independent property enables the system to be easily scaled up. The lower pressure drop reduces expenses on pressure-resistant equipment. In addition, the cheap material of membrane adsorber allows it to be disposable, which eliminate the expenses on cleaning, regeneration and sanitization [9].

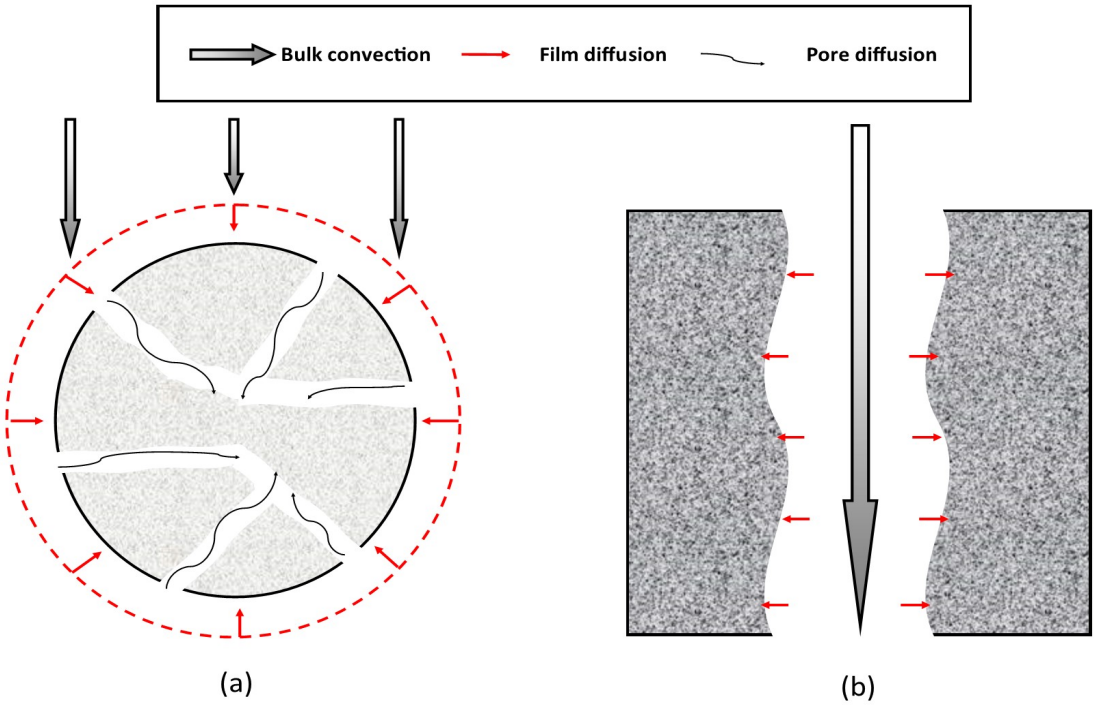

Figure 2-2 Comparison of mass transport in (a) packed-bed chromatography and (b) membrane chromatography.

Despite the advantages over column chromatography, there remain several limitations to be addressed for membrane chromatography. For membranes with non-uniform pore size distribution and thickness, the inlet flow distribution may be distorted since the feed flow will preferably go through larger pores or thinner areas. This leads to low utilization of binding sites on the membrane [9]. These drawbacks can be solved by adjusting the membrane configuration or using multiple layers for flat sheet membranes [12]. The low surface-to-bed volume ratio of membrane adsorbers results in low binding capacity, limiting its applications in the bind and elute mode where protein of interest is bound and impurities are eluted. Nevertheless, this problem has minor effect on the flow through mode of the polishing step, where impurities are bound instead and the protein flow through the membrane adsorber. In order to improve the binding capacity of the membrane adsorbers, considerable work has been done on coating pores with porous polymer to create a three-dimensional structure thus increasing the binding surface [8].

The operation of ion exchange chromatography with membrane adsorbers includes three main steps. Weak cation exchange chromatography is demonstrated as an example (Figure 2-3).

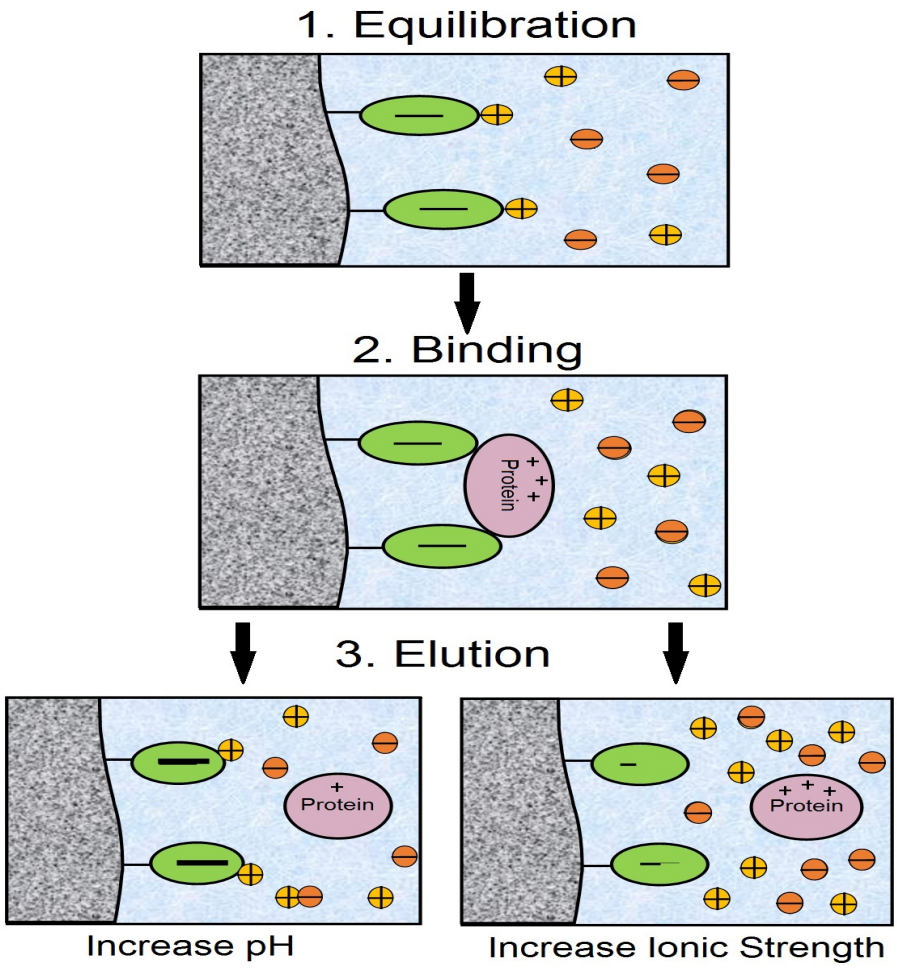

Figure 2-3 Schematic representation of protein capture with weak cation exchange membrane chromatography.

1. Equilibration: the membrane adsorber is equilibrated in the buffer with selected pH and ionic strength. This step is to make sure that the functional groups are fully ionized thus membrane is negatively charged.

2. Binding: the sample solution is prepared with the same buffer condition as in the equilibration step, so that the target protein molecules are positively charged. After adding the sample solution, protein

molecules of interest will replace counter-ions and bind on the membrane surface due to electrostatic interactions.

3. Elution: buffer conditions are altered in order to elute the bound protein. One way is to increase the pH of the buffer. At increased pH, the electrostatic interactions are disrupted since the protein becomes less positively charged, thus the protein of interest will be eluted. Another way is to elute the protein by increasing the ionic strength (salt concentration). The increased counter-ions in the solution will compete with the bound protein molecules on the membrane surface and also induce charge shielding.

2.2 Ion Exchange Membranes

2.2.1 Materials and Properties

The performance of membrane chromatography mainly relies upon the structure and chemistry of membranes. Ion exchange membranes are generally prepared in three steps: (1) selection of suitable membrane support and ligands, (2) activation of the support for immobilization of the ligands and (3) grafting of the ligands onto the activated membrane support [11].

Regenerated cellulose (RC) is the most extensively used support material for its low cost, while the short lifetime remains a problem. Compared to natural polymers, synthetic organic polymer supports have better chemical and physical stability that will increase their reusability. A variety of synthetic polymer materials are used for commercial ion exchange membranes, *e.g.* polyethersulfone (PES), polypropylene (PP), and polyvinylidene fluoride (PVDF). Some inorganic materials, *e.g.* alumina, glass fiber, and carbon nanofiber have been investigated for their high uniformity [13]. Table 2-1 lists a selection of commercial ion exchange membranes [9]. Regardless of the type of support materials employed, the following properties are always crucial: (1) pore size and pore size distribution, (2) hydrophobicity, and (3) stability.

Table 2-1 Commercial ion exchange membranes.

Manufacturer	Product name	Type	Membrane characteristics	Pore size (μm)
Millipore	Chromasorb Membrane Adsorber	Anion exchange	Polypropylene	n/a
Natrix Separations	Natrix Q	Anion exchange	Polyacrylate	0.45
	Natrix S	Cation exchange	Polyacrylate	0.45
	Natrix C	Cation exchange	Polyacrylate	0.45
Pall's Corporation	Mustang Q	Anion exchange	Modified PES	0.8
	Mustang S	Cation exchange	Modified PES	0.8
	Mustang E	Anion exchange	Modified PES	0.2
Sartorius	Sartobind Q	Anion exchange	RC	> 3
	Sartobind D	Anion exchange	RC	> 3
	Sartobind S	Cation exchange	RC	> 3
	Sartobind C	Cation exchange	RC	> 3

The functionality of ion exchange membranes comes from the ligands on the membrane surface. Membrane adsorbers can be categorized as cation exchangers and anion exchangers. Based on the ionizing strength of ligands, they can be further divided as strong cation/anion exchanger and weak cation/anion exchanger. Select ion exchange ligands are listed in Table 2-2.

Under select pH condition, cation exchange membranes have negatively charged functional groups for exchanging positive ions, while anion exchange membrane have positively charged ligands for negative ions exchange. The effect of pH on ionization of ligands is represented by the Henderson-Hasselbalch equation (Equation 2-1), where [HA] denotes the concentration of the weak acid and $[A^-]$ denotes the concentration of its conjugate base.

$$pH = pKa + \left(\frac{[A^-]}{[HA]}\right) \qquad \textbf{Equation 2-1}$$

For strong ion exchangers, the functional groups are completely ionized over a wide pH range, holding a high ion exchange capacity. For weak ion exchangers, the ionization of functional groups varies with pH.

Table 2-2 Select ligands for ion exchange membranes.

Ligand type	Ligand name	Class	Ligand structure
Cation exchanger	Sulfo (S)	Strong	$-SO_3$
	Sulfopropyl (SP)	Strong	$-CH_2CH_2CH_2SO_3$
	Carboxymethyl (CM)	Weak	$-CH_2COO^-$
Anion exchanger	Quaternary ammonium (Q)	Strong	$-N^+(CH_3)_3$
	Quaternary aminoethyl (QAE)	Strong	$-N^+(C_2H_5)_2CH_2CHOHCH_3$
	Diethylaminoethyl (DEAE)	Weak	$-CH_2CH_2N^+(C_2H_5)_2$
	Dimethylaminoethyl (DMAE)	Weak	$-CH_2CH_2N^+(CH_3)_2$

2.2.2 Natrix Weak C Cation Exchange Membrane

The weak cation exchange membrane used in this work is a Natrix C hydrogel membrane, which is comprised of a porous cross-linked polyacrylate hydrogel, physically supported by a polyolefin matrix backbone. Carboxylic acid is the functional group for ion exchange.

The grafted hydrophilic hydrogel will swell in an aqueous solution according to temperature, pH, and ionic strength, thus creating dynamic macropores [15]. The average pore size of the support matrix ranges from 0.1μm to 25μm, with the volume porosity ranging between 40% and 90%. The macroporous three-dimensional structure of the membrane allows for high permeability and high flow rate [14].

Containing a high density of carboxylate binding groups, the hydrogel membrane exhibits high binding capacity. The reported 10% breakthrough dynamic binding capacity for polyclonal human IgG was 100mg/mL at 10mV/min flow rate [14]. Zero apparent zeta potential of the membrane was observed at pH 5.3 (deionized water), indicating a pK_a value of 5.3 for Natrix C membrane [16]. According to Equation 2-1, over 50% of the carboxylic acid ligands on the membrane will be deprotonated at pH > 5.3. Thus the membrane will carry a net negative surface charge and attract positively charged protein molecules.

2.3 Model Proteins

Proteins with distinct size and charge characteristics were selected, *i.e.* lysozyme and IgG, to investigate their adsorption behavior with Natrix C.

2.3.1 Lysozyme

Lysozyme (EC 3.2.1.17) is also known as mucopeptide N-acetylmuramoylhydrolase or muramidase. In the human body, lysozyme is contained in nearly all secretions, such as tears, saliva, human milk and mucus. It has also been isolated from plants, bacteria, and bacteriophages. Hen egg white (HEW) is the major commercial source of lysozyme [17].

Lysozyme can catalyze the hydrolysis of the β-1,4-linkage between N-acetylmuramic acid and N-acetyl-D-glucosamine residues in peptidoglycans and between N-acetyl-D-glucosamine residues in chitodextrins. Therefore, lysozyme can damage the cell wall of susceptible bacteria, such as Gram-positive bacteria, which increases their permeability and causes the cells to burst [18]. In molecular biology, lysozyme is used in the alkaline-lysis procedure for extracting and isolating plasmid DNA. For its antibacterial and antifungal properties, lysozyme has also been widely used in the food industry to help prevent spoilage of foods and is classified as a food preservative in the European Union (EU).

Lysozyme is a single polypeptide chain consisting of 129 amino acid residues, with a molecular weight of ~14.3 kDa. In terms of secondary structure, it consists of 4 α-helix and 4 β-sheet conformations. Its structure is stabilized with hydrogen bonds and 4 disulfide bridges distributed in different places of the peptide chain, forming a globular shape. Lysozyme may also form electrostatic complexes with other HEW proteins, such as ovomucin, ovalbumin and ovotransferrin.

The size of lysozyme can be characterized with the hydrodynamic radius R_h, reported to be around 20 Å or 2 nm in aqueous solution [19-21]. Dismer and Hubbuch [22] proposed a hard-sphere model, which

represented lysozyme as an ellipsoid with a length of ~50 Å and a width of ~30 Å. When interacting with buffers, the size of lysozyme will be changed depending on pH and ionic strength.

With an isoelectric point (pI) of 11.3, lysozyme is positively charged at pH below its pI. Lysozyme has 29 charged groups located on the molecular surface: 11 arginine, 6 lysine, 1 histidine, 7 aspartic acid, 2 glutamic acid residues, and the N- and the C-terminus. In ion exchange chromatography, the pH condition is usually below 7, thus lysine and arginine will carry positive charges resulting in a positive net charge [23].

Lysozyme is one of the earliest characterized and most extensively studied globular proteins. The cost of lysozyme is low since it is easy to be purified from egg white. The highly compact conformation results in its small size, and with the unique pI value, making lysozyme ideal as a model protein for investigating protein capture.

2.3.2 Immunoglobulin G

Human immunoglobulins (Ig) are glycoproteins produced by plasma cells functioning as antibodies. Their general functions are antigen binding and effector binding. Igs are divided into five classes, IgA, IgD, IgE, IgM, and IgG. Type G immunoglobulin (IgG) is the most abundant antibody, about 13.5 g/L in terms of serum concentration.

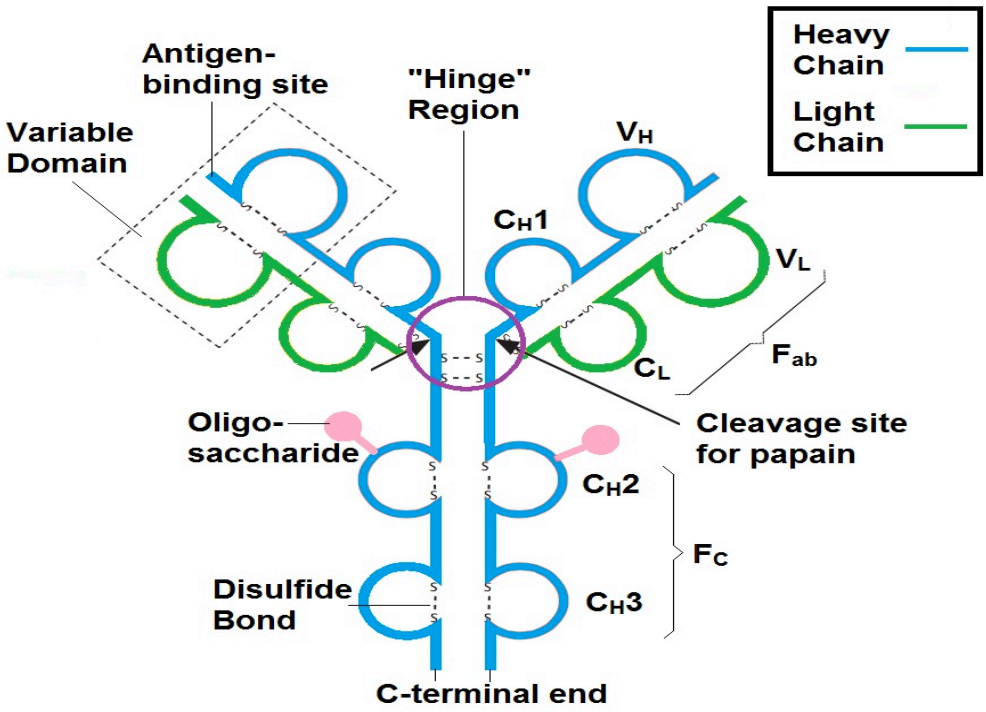

Figure 2-4 Structure of immunoglobulin G.

IgGs are "Y" shaped tetramers with two heavy chains (H) of type γ and two light chains (L) of type κ or λ [24]. IgGs can be cleaved into two F_{ab} fragments and one F_c fragment by the proteinase papain, with the F_{ab} fragment being the antigen-binding part while the F_c fragment binds to cell surfaces for interaction. IgG consists of variable regions (V) and constant regions (C), as shown in Figure 2-4. The F_c fragment consists of two constant regions, C_H2 and C_H3 for each heavy chain. The oligosaccharides are linked to the amide group of an asparagine residue in the F_c fragment through the N-glycosidic link. The disulfide bonds stabilize IgG by linking the two heavy chains together and linking the heavy chains to the light chains. They also exist within the domains to stabilize the tertiary structure. In the hinge region, IgG is greatly mobile.

The size of human IgG can be characterized by its hydrodynamic radius (R_h) or radius of gyration (R_g). The hydrodynamic radius is the radius of an equivalent hard sphere diffusing at the same rate as the molecule, determined by dynamic light scattering or other diffusion measurements [25]. A hydrodynamic radius of 5.4 nm for polyclonal human Ig was reported by Ball *et al.* [26], corresponding to a diffusion

coefficient of 4.0×10^{-7} (cm^2/s). The radius of gyration is the mass weighted average distance from the center of a molecule to each mass element in the molecule, typically obtained from static scattering measurements, small angle neutron scattering (SANS), or small angle X-ray scattering (SAXS). R_g was reported to be 4.6 nm for IgG [27].

Human IgG has a molecular weight of approximately 150kDa, with 1418 amino acid residues [28]. Human IgG (IgG1) contains 40 arginine and 46 lysine residues in its F_{ab} fragment [29], 4 lysine residues in the hinge region, and 12 arginine and 38 lysine residues in its F_c fragment [30]. Yu and Ghosh [31] investigated the binding region of human IgG with cation exchange membrane, and proposed that the $F(_{ab}')_2$ fragment after pepsin digestion was responsible for interacting with the ion exchanger.

The isoelectric point (pI) of polyclonal human IgG was determined to be in a range from 6.5 to 10 [32]. When pH is below the pI value, the surface basic residues will be ionized thus the protein molecule is positively charged. Wrzosek and Polakovic [33] reported that arginine (pK_a=12.5) and lysine (pK_a=10.8) residues on the IgG molecules were completely protonated in the pH range of adsorption experiments (pH 4 ~ pH 7), while partial histidine residues were non-ionized for its lower pK_a of 6.

Monoclonal antibodies (mAbs), produced by a single clone, have become the leading product in the biopharmaceutical industries, with at least 400 of them reported to be in clinical trials. [34] For its high biopharmaceutical value, it is essential to investigate and optimize the purification process for lowering the costs of mAb production.

2.4 Buffers for Ion Exchange Chromatography

2.4.1 Principles and Selection

In biochemistry, buffers are generally used to maintain solutions at constant pH. A buffer system consists of a weak acid (HA) and its conjugate base (A^-). The center of the buffering region is represented by the pK_a of the buffer system and the effective range is generally $pK_a \pm 1$. Typical buffers used for cation exchange chromatography are listed in Table 2-3 [35].

$$HA \Leftrightarrow H^+ + A^- \qquad \textbf{Equation 2-2}$$

Table 2-3 Common buffers for cation exchange chromatography.

Effective pH region	Buffer compounds	Counter-ion	pK_a (25°C)
1.4-2.4	Maleic acid	Na^+	1.92
2.6-3.6	Methyl malonic acid	Na^+ or Li^+	3.07
2.6-3.6	Citric acid	Na^+	3.13
3.3-4.3	Lactic acid	Na^+	3.86
3.3-4.3	Formic acid	Na^+ or Li^+	3.75
3.7-4.7	Succinic acid	Na^+	4.21
5.1-6.1	Succinic acid	Na^+	5.64
4.3-5.3	Acetic acid	Na^+ or Li^+	4.75
5.2-6.2	Methyl molonic acid	Na^+ or Li^+	5.76
5.6-6.6	2-(N-Morpholino) ethanesulfonic acid (MES)	Na^+ or Li^+	6.27
6.7-7.7	Phosphate	Na^+	7.2

The selection of buffer is critical to ion exchange chromatography, since the electrostatic interactions between the oppositely charged surface and protein are dependent on buffer conditions. In order to ensure strong electrostatic interactions between the surface and protein, the buffer pH should lie between the pK_a of the functional groups on the surface and the pI of the protein molecules. Based on this pH range, the type of buffer can be selected such that its pK_a should be within 0.7 units from the operation pH and preferably within 0.3 units [36].

The ionic strength of buffer also has a significant effect on protein adsorption due to competitive binding and shielding effects. With increased salt concentration, the counter-ions in the buffer may replace the adsorbed protein molecules and bind onto the surface. The salt ions may also shield the charged groups on the protein surface, hindering the interactions between protein molecules and binding sites on the surface. At the same pH and ionic strength condition, ionic species in the buffer may also influence protein binding. Burns and Zydney [37] proposed that the adsorption of di- and tri-valent anions led to significant reduction in the zeta potential of anion exchange membranes. Multi-valent anions were also reported to influence the surface charge of the protein through specific adsorption [38]. In addition to

ion valence, the size of counter-ions makes a difference in the competitive binding process. Faude *et al.* [38] suggested that K^+ appears to be a stronger competitor than Na^+ because of its larger size.

2.4.2 Phosphate Citrate Buffer

Phosphate buffer is among the most extensively used buffers for its high buffering capacity. Phosphate is also a natural component of biological fluids; therefore it is ideal for mimicking the biological environment. The disassociation of phosphoric acid (MW=98 g/mol) happens in three steps.

$$H_3PO_4 \leftrightarrow H_2PO_4^- + H^+ \ (pKa = 2.12) \quad \textbf{Equation 2-3}$$

$$H_2PO_4^- \leftrightarrow HPO_4^{2-} + H^+ \ (pKa = 7.21) \quad \textbf{Equation 2-4}$$

$$HPO_4^{2-} \leftrightarrow PO_4^{3-} + H^+ \ (pKa = 12.32) \quad \textbf{Equation 2-5}$$

Although phosphoric acid has three pK_a values, when used as a buffer for cation exchange chromatography, phosphate buffer is effective over a pH range from 6.7 to 7.7. During the protein capture binding step, buffer pH is preferred to be under 6.

In this work, phosphate citrate buffer is used instead for its wider effective pH ranges (pH 2 ~ pH 8). Citric acid ($C_6H_8O_7$; MW=210.1 g/mol) is a weak organic acid with three pK_a. Compared to the conventional phosphate buffer, the existence of other types of multivalent anions, *i.e.* $C_6H_6O_7^{2-}$ and $C_6H_5O_7^{3-}$, add to the complexity of the phosphate citrate buffer.

$$C_6H_8O_7 \leftrightarrow C_6H_7O_7^- + H^+ \ (pKa = 3.1) \quad \textbf{Equation 2-6}$$

$$C_6H_7O_7^- \leftrightarrow C_6H_6O_7^{2-} + H^+ \ (pKa = 4.75) \quad \textbf{Equation 2-7}$$

$$C_6H_6O_7^{2-} \leftrightarrow C_6H_5O_7^{3-} + H^+ \ (pKa = 6.4) \quad \textbf{Equation 2-8}$$

There exist several limitations with the use of phosphate citrate buffer. The presence of multi-valent anions in the phosphate citrate buffer may influence the adsorption of protein by affecting the zeta potential of membrane surface or protein molecules, as mentioned above. With a solubility of 100mg/mL in water, sodium phosphate dibasic (Na_2HPO_4) is relatively easy to crystalize and precipitate. In addition, the other component, citric acid ($C_6H_8O_7$), is a natural chemical that exists in a variety of fruits and vegetables, making it vulnerable to microbial contamination. Therefore, precautions should be taken for the storage of phosphate citrate buffer. It is recommended to store the buffer in the refrigerator and filter the impurities before usage.

2.4.3 Acetate Buffer

With a molecular weight of 60.1 g/mol, acetic acid is the second simplest carboxylic acid. It is a weak organic acid with a pK_a of 4.76 also widely used in cation exchange chromatography within its effective pH range of 4.3~5.3. There exist only mono-valent ions compared to phosphate citrate buffer.

$$CH_3COOH \leftrightarrow CH_3COO^- + H^+ \quad (pKa = 4.76) \quad \textbf{Equation 2-9}$$

With fewer constituents, acetate buffer is easier to prepare. Its solubility, chemical stability and physical stability are also higher than phosphate citrate buffer. Conductivity is another important property of buffer that may affect the protein adsorption process. Harinarayan *et al.* [39] proposed a relationship between dynamic binding capacity, pH and conductivity of buffer for mAbs with SP Sepharose FF and SP Sepharose XL in 15mM sodium acetate buffers. The conductivity for both types of buffer was measured in previous work at different pH and is given in Table 2-4.

Table 2-4 Conductivity of sodium phosphate citrate buffer and sodium acetate buffer at different pH.

pH	Conductivity (ms/cm)	
	Phosphate citrate buffer	Acetate buffer
4.5	9.79	5.92
5	11.4	9.42
5.5	12.4	12
6	13.8	12

2.5 Protein Adsorption

2.5.1 Mechanism

Protein adsorption with ion exchange chromatography depends on the net surface charge of protein molecules and the ion exchanger. The net surface charge on the adsorbent surface is determined by the ionization of functional groups with pH. As shown by the theoretical titration curve (Figure 2-5), the adsorbent will be positively charged at pH below its pK_a, and negatively charged at pH above its pK_a. Proteins are amphoteric molecules composed of amino acids, containing both weak acidic groups and basic groups. Their net surface charge will change in response to the pH of the environment. As indicated previously, the isoelectric point (pI) of a protein represents the pH at which the net surface charge on the

protein becomes zero. The protein molecules will carry positive charge at pH below its pI. Therefore, when the buffer pH is adjusted at a value between pK_a and pI, the adsorbent and protein will exhibit opposite surface net charges. Electrostatic interactions will take place and the protein molecules will adsorb to the ion exchanger. The isoelectric point generally varies from 4 to 9 for antibodies, with a majority of them over 6, making it ideal for cation exchange chromatography [40].

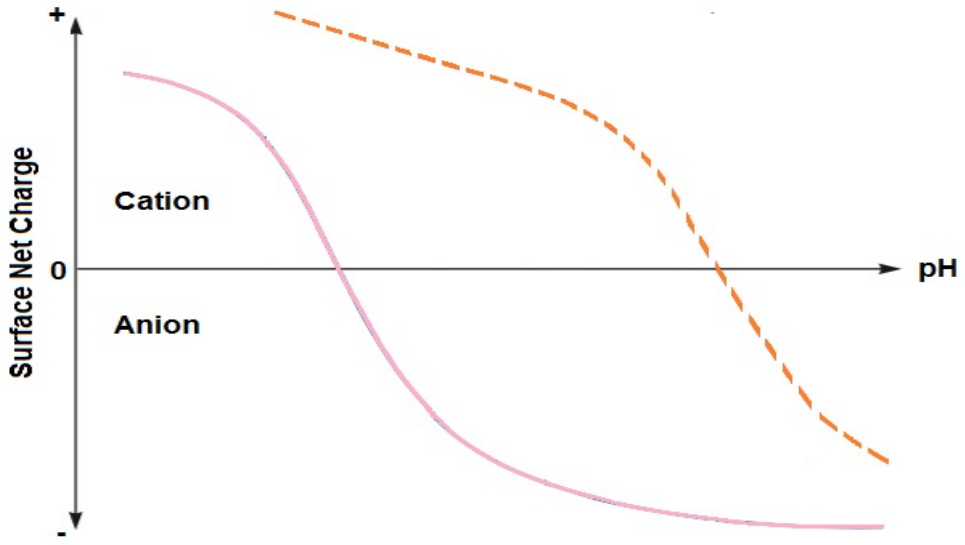

Figure 2-5 Theoretical protein titration curves, where the solid line represents the cation exchange membrane and the dash line represents the protein.

2.5.2 Adsorption Isotherms Models

Adsorption isotherms represent the retention or mobility of substance between two phases. In the context of protein capture with ion exchange chromatography, these two phases are an aqueous phase and a solid phase. Adsorption equilibrium is achieved when the adsorbate concentration in bulk solution and in solid phase is in a dynamic balance, *i.e.* the adsorbate concentration is constant while there is still exchange between the two phases, after sufficient time. A mathematical relationship representing the adsorption process can be developed from the adsorbate concentration on the solid phase against the adsorbate equilibrium concentration in solution. Equilibrium isotherm models are generally formulated under three fundamental considerations, kinetic, thermodynamics and potential theory. Among the isotherm models

developed through the years, the Langmuir model and the steric-mass action model have been used for the analysis of protein adsorption on ion exchange chromatography surfaces [41, 42].

In order to improve time efficiency and reduce operational cost, it is essential to predict the protein purification process using adsorption models. In recent years, the progresses in algorithms and calculation power have catalyzed the use of modeling for optimization of chromatographic steps.

2.5.2.1 Langmuir Model

The Langmuir model is the simplest and the most extensively used adsorption model for fluid-solid interphases. It is formulated based on several assumptions: (1) monolayer adsorption, the adsorbed layer is only one molecule in thickness, (2) homogeneous surface, the binding sites are identical and finite, (3) homogeneous adsorption, all molecules and sites are energetically identical and (4) no lateral interaction and steric hindrance between the adsorbed molecules [43]. The assumptions usually hold true when the binding site density is so low that the average distance between adjacent sites is larger than the diameter of the adsorbed molecule.

The equilibrium reaction for monolayer adsorption can be represented as follows [44],

$$\boldsymbol{P + S \Leftrightarrow PS} \quad \textbf{Equation 2-10}$$

where P represents the protein molecules in the mobile phase, S represents available binding sites on the membrane surface and PS represents adsorbed protein molecules on the sites. Let k_1 be the adsorption constant and k_{-1} be the desorption constant. Hence the rate of change of the adsorbed protein concentration is given by,

$$\boldsymbol{\frac{dq}{dt} = k_1 C_p (q_{max} - q) - k_{-1} q} \quad \textbf{Equation 2-11}$$

where C_p is the protein concentration in solution (mg/mL), q is the adsorbed protein concentration (mg/mL), q_{max} is the maximum binding capacity (mg/mL), and t is the time (s). At equilibrium, Equation 2-11 equals to zero and can be rearranged as,

$$\boldsymbol{q_e = \frac{C_e\, q_{max}}{C_e + \frac{k_{-1}}{k_1}}} \quad \textbf{Equation 2-12}$$

where C_e is the equilibrium protein concentration (mg/mL) and q_e is the adsorbed protein concentration at equilibrium or the binding capacity (mg/mL). Substituting $\frac{1}{K} = \frac{k_{-1}}{k_1}$ into Equation 2-12 gives the mathematical expression for the Langmuir adsorption model,

$$q_e = \frac{q_{max}\, K\, C_e}{1 + K\, C_e} \quad \textbf{Equation 2-13}$$

where equilibrium constant K is the ratio of adsorption rate over desorption (mL/mg). Other adaption of the model is given as Equation 2-15, where the dissociation constant K_d (K_d=1/K) is used instead of K.

$$q_e = \frac{q_{max}\, C_e}{C_e + K_d} \quad \textbf{Equation 2-14}$$

The two parameters in the Langmuir model are the maximum binding capacity (q_{max}) and the equilibrium constant (K). q_{max} denotes the maximum amount of protein that can be adsorbed onto the adsorbent surface, graphically represented by the plateau after the equilibrium saturation point. K denotes the adsorption affinity, represented by the initial slope of the linear portion of the adsorption isotherm. The parameters for the Langmuir adsorption model are usually estimated from batch static protein binding experiments. The Langmuir model can be linearized as follows [45],

$$\frac{1}{q_e} = \left(\frac{1}{q_{max}\, K}\right)\frac{1}{C_e} + \frac{1}{q_{max}} \quad \textbf{Equation 2-15}$$

By plotting $1/q_e$ against $1/C_e$, the maximum binding capacity and the equilibrium constant can be determined from the intercept and the slope of the plot. However, rearranging the Langmuir model may disturb the error structure of the linear regression equation. The order of magnitude for error of the original Langmuir model is 0 or 1, while the order of magnitude for error of the linearized model is -3 or -2. Therefore, it is preferable to fit the equilibrium protein concentration and equilibrium adsorption into the original Langmuir model, and employ the least squares approach for non-linear regression [46]. In terms of dynamic protein binding experiments, the following dimensionless Langmuir kinetics equation is considered [47],

$$R_A = \frac{n'}{q'} C_i (1 - C_s) - \frac{n'}{q'(r-1)} C_s \quad \textbf{Equation 2-16}$$

where R_A is the dimensionless reaction rate by adsorption, n' is the dimensionless number of transfer units, q' is the dimensionless saturation capacity, C_i is dimensionless interfacial solute concentration in the liquid phase, C_s is the dimensionless solute concentration in the solid phase, and r is the dimensionless separation factor. Different regression methods may result in variations in parameter estimations.

The Langmuir model has been widely used for understanding the mechanism of protein adsorption in ion exchange chromatography, especially for lysozyme, a small protein.

2.5.2.2 Steric Mass-Action Model

A number of adsorption models for the description of the ion-exchange adsorption equilibrium have been suggested over the past few decades. Prompted by the observation of protein with zero net charge binding onto the anion and cation exchangers [48], the steric mass-action (SMA) model (Figure 2-6) was developed. In the 1990s, the steric mass-action model for protein adsorption with ion exchange chromatography was first proposed by Brooks and Cramer [49], and combined the stoichiometric displacement model (SDM) [48, 50, 51] and the steric hindrance of salt [52].

The model was developed based on the following assumptions: (1) the stationary and mobile phases are thermodynamically ideal, (2) the multi-pointed binding of protein can be explained by its characteristic charge, (3) competitive binding can be represented by mass-action equilibrium, (4) the steric hindrance of salt counter-ions is caused by adsorption of large macromolecules, (5) the effect of co-ions can be neglected and (6) equilibrium parameters are not dependent on solute or salt concentration.

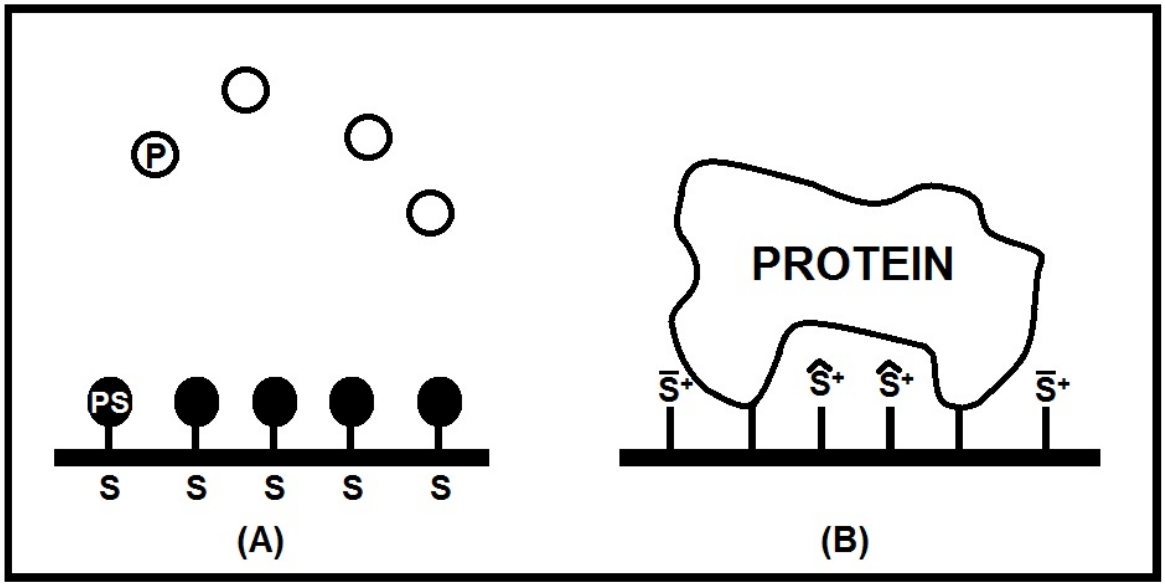

Figure 2-6 Schematic illustration of the adsorption of a protein molecule: (A) Langmuir model, where P denotes free protein molecules, PS denotes absorbed protein molecules, and S denotes binding sites; (B) steric mass-action (SMA) model, where $\hat{S}^+$ denotes the sterically hindered salt counter-ions and $\bar{S}^+$ denotes the non-sterically hindered counter-ions.

The SMA model considers various effects within the ion-exchange adsorption equilibrium, *i.e.* the salt dependency, the local charge region, the steric effects and the size of the protein molecule. It has been

reported to successfully predict complex chromatographic behavior of proteins in gradient and displacement ion-exchange systems [53-55]. For single component equilibrium, the stoichiometric exchange of the protein and salt counter-ions can be described by,

$$\mathbf{C_e + \nu\, \overline{q_s} \Leftrightarrow q_e + \nu\, C_s} \qquad \textbf{Equation 2-17}$$

where C_e and q_e are protein concentrations in the mobile phase and stationary phase respectively (mmol/L), C_s and $\overline{q_s}$ are salt concentrations in the mobile phase and stationary phase (mmol/L) respectively. The overscore indicates that the salt counter-ions are exchangeable with the protein. ν is the characteristic charge of protein. The equilibrium constant K_a for SMA model is then defined as,

$$\boldsymbol{K_a = \left(\frac{q_e}{C_e}\right)\left(\frac{C_s}{\overline{q_s}}\right)^{\nu}} \qquad \textbf{Equation 2-18}$$

The total salt concentration on the stationary phase after protein adsorption is given by the sum of $\overline{q_s}$ and the concentration of salt counter-ions that are hindered by adsorbed proteins, which can be represented by the steric factor σ of the protein,

$$\boldsymbol{q_s = \overline{q_s} + \sigma q_e} \qquad \textbf{Equation 2-19}$$

Along with the electroneutrality on the stationary phase given by ion exchange capacity Λ (mmol/L),

$$\boldsymbol{\Lambda = \overline{q_s} + (\nu + \sigma) q_e} \qquad \textbf{Equation 2-20}$$

The SMA isotherm can be derived by substituting Equation 2-20 into Equation 2-18,

$$\boldsymbol{C_e = \left(\frac{q_e}{K_a}\right)\left(\frac{C_s}{\Lambda - (\nu+\sigma) q_e}\right)^{\nu}} \qquad \textbf{Equation 2-21}$$

The parameters to be estimated in the SMA model are the equilibrium constant (K_a), the ratio of the adsorption and desorption coefficients; the characteristic charge (ν), the number of sites on the protein that actually interact with the ion exchanger and the steric factor (σ), the number of sites on the adsorbent surface that are shielded by the protein and are prevented from exchange with protein in free solution. The ion exchange capacity (Λ) is an indication of the number of active binding sites on the membrane, which can be determined experimentally. The salt concentration (C_s) is the concentration of salt counter-ions in the mobile phase at equilibrium, determined through various methods in the literature. It was defined as the salt concentration of buffer at breakthrough for dynamic method. Karlsson *et al.* [40] established a linear relationship between the conductivity and salt concentration, thus the salt concentration of buffer can be calculated from the conductivity. For static method, C_s is assumed to be the initial concentration of

salt counter-ions in the buffer, calculated by adding the equivalent concentration of counter-ions in the buffer with the added salt concentration [56].

The parameters for the SMA model can be determined by static and dynamic protein binding experiments. For static protein binding experiments, batch adsorption experiment is applied to measure the equilibrium binding capacity [56]. The experimental equilibrium protein concentration and equilibrium binding capacity can be fitted into the SMA model with MATLAB and parameters are estimated together with the least squares approach. For dynamic protein binding experiments, gradient chromatographic experiments [49] are carried out for the determination of K_a and ν, where the retention time is measured to create a straight line of the logarithmic retention time against the logarithmic salt concentration. The slope of the line is the characteristic charge, and the intercept gives the equilibrium constant. Frontal chromatographic experiments are applied for the determination of steric factor. The steric factor can be estimated from experimental data at high protein concentration. Osberghaus *et al.* [57] proposed another parameter estimation approach based on an inverse method and a mechanistic model, where both retention times and complete elution profiles can be predicted.

Chapter 3
Experiments and Results

3.1 Introduction

Applications of chromatography in protein purification [8] and monoclonal antibody purification [4, 9, 11] have been reviewed for affinity, ion exchange, and hydrophobic interaction and reversed-phase based separations, where affinity separation takes up about 55% of all usage. However, the low throughput and poor bed utilization limited the development of Protein A affinity chromatography [1]. Ion exchange membrane chromatography has been reported as a potential alternative.

The effect of properties of the ion exchanger on protein adsorption have been extensively investigated in the literature, where ligand type [58], ligand density [59], pore size [60] and pore structure [61, 62] are reported to be significant factor for achieving high binding capacity. The ion exchanger investigated were ion exchange resins or Sartobind membranes, while studies on Natrix membranes haven't been reported. Several groups have studied the effect of buffer on protein capture with ion exchange chromatography, while most of them limited their work to the effect of pH and ionic strength [23, 33, 63, 64], neglecting the effect of ion composition.

In this work, buffer effects on the properties of Natrix C and protein capture with lysozyme and IgG will be discussed. The significance of ion composition and buffer conditions will be investigated in details for phosphate citrate buffer and acetate buffer. This chapter is formatted for submission to the Journal of Chromatography A.

3.2 Materials and Methods

3.2.1 Materials

Weak cation exchange membrane, Natrix HD-C hydrogel membrane (diameter: 25 mm and 47 mm) was provided by Natrix Separations Inc. (Burlington, Ontario, Canada). Model proteins were human immunoglobulin G (IgG), purchased from Equitech-Bio, Inc. (Kerrville, Texas, USA) and lysozyme chloride, provided by Neova Technologies (Abbotsford, British Columbia, Canada).

All buffers and solutions were prepared using Milli-Q water, obtained from a Millipore Synergy UV system (EMD Millipore, Darmstadt, Germany). Sodium phosphate citrate buffer was prepared by mixing 0.1M citric acid, anhydrous (EMD Chemicals Inc., Gibbstown, USA) and 0.2M sodium phosphate dibasic

heptahydrate (Fisher Scientific, Fair Lawn, USA). Sodium acetate buffer was prepared by mixing 0.2 M acetic acid, glacial (EMD Chemicals Inc., Gibbstown, USA) and 0.2 M sodium acetate (EMD Chemicals Inc., Gibbstown, USA). Phosphate buffer was prepared with monosodium phosphate monohydrate (BDH Inc., Toronto, Canada) and sodium phosphate dibasic heptahydrate.

Potassium chloride (EMD Chemicals Inc., Gibbstown, USA) was added into the phosphate citrate buffer and acetate buffer to achieve a salt concentration of 0.1 M, 0.3 M, and 1 M, for measuring membrane swelling. Sodium chloride (BDH Inc., Toronto, Canada) was added into the phosphate citrate buffer and acetate buffer to achieve a salt concentration of 50 mM and 100 mM, for measuring static protein binding capacity.

3.2.2 Membrane Swelling

Each membrane disc (diameter=25 mm) was cut into eight pieces and the dry weight of each piece was measured. Each membrane piece was I ersed in 20 mL buffer with certain pH and ionic strength in a vial. The membrane pieces were equilibrated on a shaker (Thermo Scientific 2309 lab rotator, Canada) for 4 hours. After the equilibration, the membrane pieces were removed and hanged for 10 min before the wet weight was measured. All experiments were run in triplicate at room temperature and room humidity was recorded with a thermo-hygrometer (Smart^2, InterTAN, Barrie, Canada).

The swelling factor q_{ms} was calculated from the following equation,

$$\mathbf{q_{ms} = \frac{m_{swollen}}{m_{dry}}} \qquad \textbf{Equation 3-1}$$

where $m_{swollen}$ is the mass of the wet membrane (g) and m_{dry} is the mass of the dry membrane (g).

3.2.3 Environmental Scanning Electron Microscopy (ESEM)

The pore structures of the native dry Natrix C membrane, and buffer equilibrated and subsequently freeze-dried membrane are visualized with Field Emission Gun Environmental Scanning Electron Microscope (FEG-ESEM, Quanta 250, FEI company, Netherlands), at low vacuum mode. The magnification was 1000 x and 5000 x. The ESEM images were qualitatively analyzed.

Membrane samples (5 mm × 5 mm) were prepared by equilibrating in phosphate citrate buffer at pH 5 and pH 7 with 0 M and 1 M KCl, and acetate buffer at pH 5 with 0 M and 1 M KCl for 24 hours while being shaken at 80 rpm. The samples were subsequently freeze-dried (Epsilon1-4, Martin Christ, Germany) for 22 hours.

3.2.4 Static Protein Adsorption Capacity

Static protein adsorption capacity was obtained from batch adsorption experiments. Binding buffer was prepared by dissolving IgG and lysozyme in plain phosphate citrate buffer or acetate buffer to obtain a series of protein concentrations (0.1 mg/mL~4 mg/mL). 50 mM and 100 mM NaCl was added to adjust the ionic strength of buffers. A series of protein standard was prepared by dissolving lysozyme and/or IgG in plain buffer at pH 5 and in buffer at pH 5 with 50 mM, 100 mM NaCl. The concentration of protein standards ranged from 0.05 mg/mL to 4 mg/mL. For buffer with added NaCl, the pH was adjusted again to reach pH 5.

Each membrane disc was cut into eight pieces and weighed. Each piece was equilibrated for 2 hours in 5 mL pH 5 phosphate citrate buffer or pH 5 acetate buffer in a vial on the shaker (Thermo Scientific 2309 lab rotator, Canada). After equilibration, 5 mL binding buffer with protein concentration range from 0.1 mg/mL to 4 mg/mL were added to each vial and incubated on shaker for 24 hours for IgG, or 72 hours for lysozyme, to achieve equilibrium binding. Triplicates were performed for each protein concentration. All experiments were run at room temperature. The final solutions were filtered through a 0.45 μm PES syringe filter (Thermo Scientific, Ottawa, ON, Canada).

The calibration curve was prepared by measuring the ultraviolet (UV) absorbance of a series of protein standards at 280 nm using a UV spectrophotometer (Spectronic Gensys 5, Thermo Scientific, Waltham, USA). A linear relationship between the UV absorbance and the protein concentration was established for each buffer condition. Final protein concentration was thus determined from UV absorbance at 280 nm. Assuming that the volume of the solution remained constant during the binding process, the static binding capacity (or adsorbed protein concentration at equilibrium) was calculated as follows,

$$q_e = (C_0 - C_e) * (\frac{V_{solution}}{V_{membrane}}) \qquad \textbf{Equation 3-2}$$

where q_e is the static binding capacity (mg/ mL); C_0 is the initial protein concentration when binding started (mg/mL); C_e is the equilibrium protein concentration (mg/mL); $V_{solution}$ is the total volume of binding buffer (mL), 10 mL in this experiment; $V_{membrane}$ is the volume of the membrane piece (mL), calculated from the mass ratio of the membrane piece and the whole membrane. The volume of the whole membrane was assumed to be constant, and equals 0.477 mL.

The procedure was repeated for IgG in pH 5 phosphate citrate buffer with 50 mM and 100 mM NaCl, and in pH 5 acetate buffer with 50 mM and 100 mM NaCl respectively.

3.2.5 Dynamic Protein Adsorption Capacity

Dynamic binding experiments were conducted using an ÄKTA prime^{TM} system (GE Healthcare, Sweden) for lysozyme and IgG. The UV detector was set at 280 nm. The dead volume of the system was 3.38±0.21 mL, determined by measuring the change in conductivity of 0.1 M NaOH at a flow rate of 2 mL/min. The type of membrane used was Natrix C (diameter=25 mm). Each run used a fresh membrane.

After washing all the lines with 20% ethanol solution and deionized water, each line was flushed with corresponding buffers at a flow rate of 5 mL/min to determine the absorbance of feed protein concentration A_0 at 280 nm. One membrane disc was then inserted into the membrane holder and attached to the system before starting the dynamic binding experiment (Table 3-1).

Table 3-1 Steps of dynamic binding experiments with ÄKTA system.

Time (min)	Function	Flow rate (mL/min)
10	Equilibration	1
50	Binding	1
20	Washing	1
20	Elution	2

The equilibration step prepares the membrane for binding by exposing it to phosphate citrate buffer or acetate buffer with certain pH (4.8 or 5). The binding step exposes the column to protein solution (0.5 mg/mL or 2 mg/mL). The washing step washes off any protein that was weakly bound on the membrane surface using same buffer as that of the equilibration step. The elution step elutes the adsorbed protein with buffer at higher ionic strength and/or higher pH depending on type of binding buffer. For phosphate citrate buffer, pH 7 phosphate citrate buffer with 1M KCl was used as the elution buffer. For acetate buffer, pH 5 phosphate buffer with 1M KCl was used as the elution buffer.

The data were exported and analyzed with MATLAB (R2014a). Breakthrough curves and full chromatograms were generated with MATLAB. The dynamic binding capacity at 10% breakthrough ($DBC_{10\%}$) was calculated (Equation 3-3) from the breakthrough curve at 10% breakthrough point, *i.e.* 10% of the absorbance of feed protein solution (A_0) was detected from the effluent.

$$\boldsymbol{DBC = \frac{C_{po} \times V_{permeate}}{V_{membrane}}} \quad \textbf{Equation 3-3}$$

where C_{po} is the feed protein concentration (mg/mL); $V_{permeate}$ is the volume of the permeate (mL), calculate by the time (min) at 10% breakthrough point multiply the flow rate (mL/min); $V_{membrane}$ is the volume of the membrane (mL), which was assumed to be constant and equals 0.1mL.

A 2^2 factorial design (Table 3-2) was conducted to investigate the effect of binding buffer condition, buffer pH and feed protein concentration, on dynamic protein binding for lysozyme with phosphate citrate buffer, where + denotes condition at a high level and – denotes condition at a low level. The elution buffer used was phosphate citrate buffer at pH 7 with 1M KCl.

Table 3-2 2^2 Factorial design for investigating the condition of binding buffer.

Level	+	-
Buffer pH	5	4.8
Feed protein concentration (mg/mL)	2	0.5

3.2.6 Protein Adsorption Models

The data collected from the static protein adsorption experiment were fitted into the Langmuir model (Equation 2-13) and the steric mass-action (SMA) model (Equation 2-21). The two Langmuir parameters, q_{max} and K, were estimated with the least squares approach (MATLAB, R2014a) by minimizing the following equation,

$$(q_a - q)^2 = \left(q_a - \frac{q_{max}\, K\, C_e}{1 + K\, C_e}\right)^2 \qquad \textbf{Equation 3-4}$$

where q_a is the experimental static binding capacity at equilibrium (mg/mL); q is the estimated static binding capacity from the Langmuir model (mg/mL); C_e is the equilibrium protein concentration (mg/mL); q_{max} is the maximum binding capacity (mg/mL); K is the Langmuir equilibrium constant (mL/mg), the ratio of adsorption rate to desorption rate. The adjusted coefficient of determination R^2_{adj} was used as an indicator of goodness of fit for the Langmuir model, calculated with the Curve Fitting Toolbox within MATLAB.

$$R^2_{adj} = 1 - \left(\frac{n-1}{n-p}\right)\left(1 - \frac{SS_R}{SS_E}\right) \qquad \textbf{Equation 3-5}$$

where n is the number of observations; p is the number of parameters; SS_R is the sum of squares of regression; SS_E is the sum of squares of error. R^2_{adj} is the adjusted R^2 statistics, which indicates the

percentage of variation present in the data accounted for by the model and keeps constant with increased variables in the model [65].

The SMA model contains the ion exchange capacity (Λ), the salt counter-ions concentration (C_s), the equilibrium constant (K_a), the characteristic charge (ν), and the steric factor (σ). The ion exchange capacity A was obtained by titration method from previous work as 204.24 mM. The salt counter-ion (Na^+) concentration is 206 mM in pH 5 phosphate citrate buffer and 140 mM in pH 5 acetate buffer. With 50 mM and 100 mM NaCl added, the salt concentration C_s becomes 256 mM and 306 mM for phosphate citrate buffer and 190 mM and 240 mM for acetate buffer. The three remaining parameters can be estimated with the least squares approach with MATLAB. Equation 3-5 was minimized, where C_a is the experimental equilibrium protein concentration (mM), C_e is the estimated protein concentration from the SMA model (mM), and q_e is the experimental static binding capacity (mM).

$$(C_a - C_e)^2 = \left[C_a - \left(\frac{q_e}{K_a}\right)\left(\frac{C_s}{\Lambda-(\nu+\sigma)q}\right)^{\nu}\right]^2 \qquad \textbf{Equation 3-6}$$

The coefficient of determination R^2 was used as the indicator of goodness of fit.

$$R^2 = 1 - \frac{SS_E}{SS_T} = \frac{SS_R}{SS_T} \qquad \textbf{Equation 3-7}$$

where SS_T is the total sum of squares.

3.2.7 Statistical Analysis

Paired two sample t-test analyses were performed to determine the significance of difference between mean values of two sample sets. The test statistics t_0 was calculated as follows,

$$t_0 = \frac{\bar{d}}{S_d/\sqrt{n}} \qquad \textbf{Equation 3-8}$$

where $\bar{d}$ is the sample mean of the differences,

$$\bar{d} = \frac{1}{n}\sum_{j=1}^{n} d_j \qquad \textbf{Equation 3-9}$$

and S_d is the sample standard deviation of the differences,

$$S_d = \left[\frac{\sum_{j=1}^{n}(d_j-\bar{d})^2}{n-1}\right]^{1/2} \qquad \textbf{Equation 3-10}$$

The hypothesis H_0: $\mu_d=0$ would be rejected if,

$$|t_0| > t_{\frac{\alpha}{2},n-1} \qquad \textbf{Equation 3-11}$$

where $t_{\frac{\alpha}{2},n-1}$ is the upper α/2 percentage point of the t distribution with n-1 degrees of freedom. 95% confidence interval was used in this work.

An analysis of variance (ANOVA) was performed to determine the significance of factors or their interactions, for two-factor factorial designs with n replicates (n=3). It assumes that errors are normally and independently distributed with constant variance. The factors were denoted as factor A with a levels and factor B with b levels. The total variability in the data can be partitioned into,

$$SS_T = SS_A + SS_B + SS_{AB} + SS_E \quad \textbf{Equation 3-12}$$

where SS_T is the total corrected sum of squares, SS_A is the sum of squares of factor A, SS_B is the sum of squares of factor B, SS_{AB} is the sum of squares of the interaction between factor A and factor B, and SS_E is the sum of squares of error. The mean square (MS) can be obtained by divide each sum of squares by its degrees of freedom. The test statistics F_0 was calculated as follows,

$$F_0 = \frac{MS_0}{MS_E} \qquad \textbf{Equation 3-13}$$

The hypothesis that the effect of A, B, or AB is not significant would be rejected if,

$$F_0 > F_{\alpha,\upsilon 1,\upsilon 2} \quad \textbf{Equation 3-14}$$

where υ1 is the degree of freedom of A, B, or AB, and υ2 is the degree of freedom of error. 95% confidence interval was used in this work. The test procedure was summarized in an analysis of variance table, as shown in Table 3-3.

Table 3-3 The analysis of variance table.

Source of variation	Sum of squares	Degrees of freedom	Mean Square	F_0	$F_{\alpha, \upsilon 1, \upsilon 2}$
Factor A	SS_A	a-1	$\boldsymbol{MS_A = \frac{SS_A}{a-1}}$	$\boldsymbol{\frac{MS_A}{MS_E}}$	-
Factor B	SS_B	b-1	$\boldsymbol{MS_B = \frac{SS_B}{b-1}}$	$\boldsymbol{\frac{MS_B}{MS_E}}$	-
Interaction AB	SS_{AB}	(a-1)(b-1)	$\boldsymbol{MS_{AB} = \frac{SS_{AB}}{(a-1)(b-1)}}$	$\boldsymbol{\frac{MS_{AB}}{MS_E}}$	-
Error	SS_E	ab(n-1)	$\boldsymbol{MS_E = \frac{SS_E}{ab(n-1)}}$		
Total	SS_T	abn-1			

3.3 Results and Discussion

3.3.1 Effect of Buffer on Membrane Properties

3.3.1.1 Effect of Buffer on Membrane Swelling

The Natrix C membrane consists of a flexible polyolefin support and a porous functionalized hydrogel layer, presenting three-dimensional open pores with nominal pore size of 0.3 μm [14]. When interacting with buffer solution, the membrane will exhibit swelling behavior in response to different buffer conditions, such as pH and ionic strength. Membrane swelling alters pore size and affects the availability of binding sites, which will further affect protein binding and recovery. Therefore it is important to investigate the effect of buffer on membrane swelling.

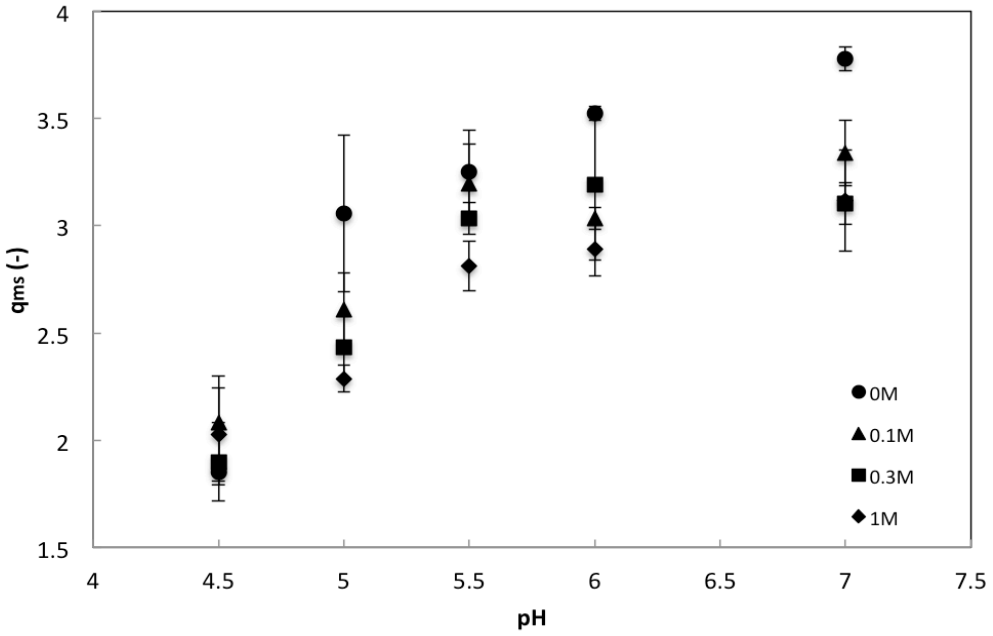

(A)

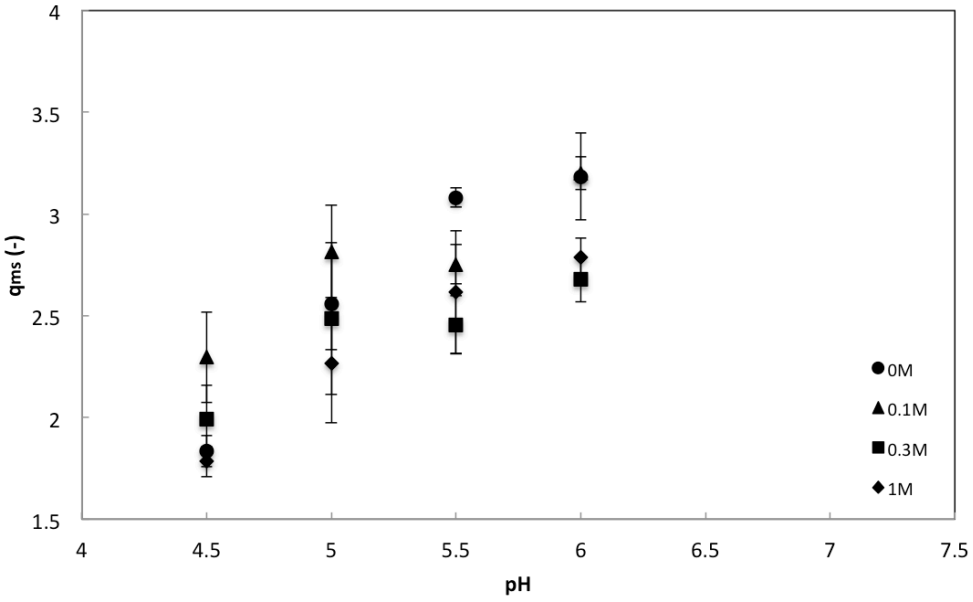

(B)

Figure 3-1 Swelling factor of Natrix C membrane in (A) phosphate citrate buffer and (B) acetate buffer at various pH and ionic strength (KCl concentration). Error bars represent standard error (n=3).

The swelling behavior of Natrix C hydrogel membrane was investigated in phosphate citrate buffer with a pH range of 4.5 to 7 and an ionic strength (KCl concentration) range of 0M to 1M. (Figure 3-1 A) The swelling factor q_{ms} ranged from 1.85 (pH 4.5; 0 M) to 3.78 (pH 7; 0 M), smaller than values measured by Hassel [16] for the same Natrix C membrane in phosphate citrate buffer where q_{ms} was 3.4 (pH 4.5; 0 M) and 4.53 (pH 7; 0 M). The difference in results may come from sensitivity of the method to environmental humidity and time. Comparable values were also reported by Yarimkaya and Basan for polyacrylate hydrogel materials in phosphate buffer [66].

The effect of pH on membrane swelling was statistically significant, evaluated by analysis of variance (ANOVA) at 95% confidence. At constant ionic strength, the swelling factor initially increased significantly with pH, and then leveled off after pH 6.0. When pH was increased from 4.5 to 7, the swelling factor increased 104% at 0 M KCl and 43% at 1M KCl. The swelling behavior can be explained by the composition of the membrane, which contains porous polyacrylate hydrogel with pendant carboxylic binding groups that exhibit variable ionization according to pH condition. The effect of pH on membrane swelling is mainly due to electrostatic repulsion. With a pK_a of 5.3 [16], the carboxylic acid ligands on the membrane will be ionized and negatively charged at pH>5.3. The increasing negative surface charge of membrane with pH leads to strong repulsion within the polymer network, thus the polymer chain tends to uncoil and allows more water molecules to be attracted to the hydrophilic carboxylic group. While at pH 6.0, the pores of hydrogel almost reached its maximum size, thus further increase of pH would not influence the swelling factor.

The influence of ionic strength on swelling was also statistically significant, evaluated by analysis of variance (ANOVA) test with 95% confidence. Even though its interaction with pH was statistically determined to be insignificant with a strict confidence region (95%), the effect of ionic strength on swelling factor did appear to be dependent on buffer pH. In general, the swelling factor decreased with ionic strength at constant pH. While at pH 4.5, the swelling factor slightly increased (9.5%) with ionic strength increasing from 0M to 1M. The most pronounced effect of ionic strength on swelling factor was observed at pH 5, with a reduction of 25%. The effect of buffer ionic strength on membrane swelling mainly comes from osmosis. Osmotic pressure is the driving force of the penetration of water into the hydrogel, determined by the following equation [67],

$$\Pi = \frac{RT}{V_W} \ln \frac{\bar{a}_W}{a_W} \qquad \textbf{Equation 3-15}$$

where R is the gas constant (L atm/K mol); T is the thermodynamic temperature; V_W is the molar volume (m^3/mol); $\bar{a}_W$ and a_W are the activities of solvent in the solution and in the membrane phase. According to the Donnan osmotic pressure equilibrium, an increase in counter-ions in the mobile phase will decrease the osmotic pressure within the hydrogel and cause the shrinkage of the hydrogel [68]. The ionic strength of the buffer was increased by introducing K^+ in the solution, which lowered the difference of ion concentration between the solution and the hydrogel. Therefore, the lowered osmotic pressure suppressed the diffusion of water molecule into the hydrogel, resulting in the reduction of the swelling factor with higher ionic strength.

The buffer ionic strength also influenced the swelling behavior of membrane by alleviating the electrostatic repulsion. The increase of K^+ in solution reduces the negative surface charge of membrane and the polymer chain tends to be coiled, thus the hydrophilic domain is restricted and less water was adsorbed. It is also proposed that steric hindrance may be an explanation for the salt effect on swelling [69], where the presence of K^+ restricted the binding of water molecules.

The membrane swelling with phosphate citrate buffer confirmed that both pH and ionic strength of buffer have a significant influence on membrane swelling. The swelling factor was found to increase with pH and decrease with ionic strength, which agrees with the observation from Chan and Neufeld [15] for semisynthetic network alginate polymer (SNAP) hydrogel in NaCl solutions.

In order to investigate the effect of ion content on membrane swelling, the swelling factor of the membrane in acetate buffer with a pH range of 4.5 to 6 and an ionic strength range of 0M to 1M was measured. The swelling factor in acetate buffer ranged from 1.78 to 3.20, at room humidity of 33%. The swelling factor also increased with pH and decreased with ionic strength, exhibiting similar trend as in phosphate citrate buffer. The significance of pH effect and ionic effect were verified by ANOVA. Nevertheless, the effect of pH and ionic strength appeared to be milder in acetate buffer than in phosphate citrate buffer. When pH was increased from 4.5 to 6, the swelling factor increased 73% and 40% in acetate buffer with an ionic strength of 0M and 1M respectively, compared to 91% and 46% for phosphate citrate buffer. At a constant pH of 5, the swelling factor decreased 11% with an increase of ionic strength from 0M to 1M in acetate buffer; in contrast the increase was 25% in phosphate citrate buffer.

Paired t-test (95% confidence) were performed and concluded that there are no significant difference of swelling factors between the two types of buffer, even though the ion content was different: phosphate citrate buffer contains multivalent anions while acetate buffer contains only monovalent ions. Multivalent

anions may reduce the zeta potential of positively charged membrane/protein by specific adsorption, however, their effect on the surface charge of membranes with weakly acidic carboxylic or phenolic groups is small [37].

The interaction between buffer and membrane was evaluated through membrane swelling. Both pH and ionic strength showed significant influence on swelling, where the swelling factor increased with pH and decreased with ionic strength in the two types of buffer. The difference of ion content between phosphate citrate buffer and acetate buffer did not significantly influence the swelling factor. The results were verified with statistical analysis.

Membrane swelling was expected to make a change in pore size and distribution, which led to investigating the membrane with scanning electron microscope. In order to further understand the effect of pH, ionic strength and ion content on cation exchange chromatography, interactions within buffer, membrane and protein are further investigated through static binding and dynamic binding.

3.3.1.2 Membrane Surface Characterization by Environmental Scanning Electron Microscopy (ESEM)

The membrane surface morphology and pore morphology was investigated by ESEM. Figure 3-2 (A) illustrates the irregular, complex structure of Natrix C membrane, physically supported by interlaced thin fibers and filled with functionalized hydrogel. Figure 3-2 (B) showcases the structure of macropores of the dry membrane, with diverse pore size. The microstructure of the buffer equilibrated and subsequently freeze-dried membrane is presented in Figure 3-2 (C), where the hydrogel content increased and covered the support fibers. By qualitative comparison between Figure 3-2 (B) and Figure 3-2 (D), it was observed that the pore size of the buffer equilibrated membrane with pH 7 phosphate citrate buffer was smaller than the native membrane, indicating the significant effect of the hydrogel component. Average pore size and the pore size distribution could not be quantitatively characterized due to difficulties in properly defining pore contours with the current image analysis system. It is proposed that a combination of characterization methods should be considered for appropriate pore structure characterization: liquid impregnation method, batch size-exclusion method, inverse size-exclusion chromatography, and permeability measurement [61].

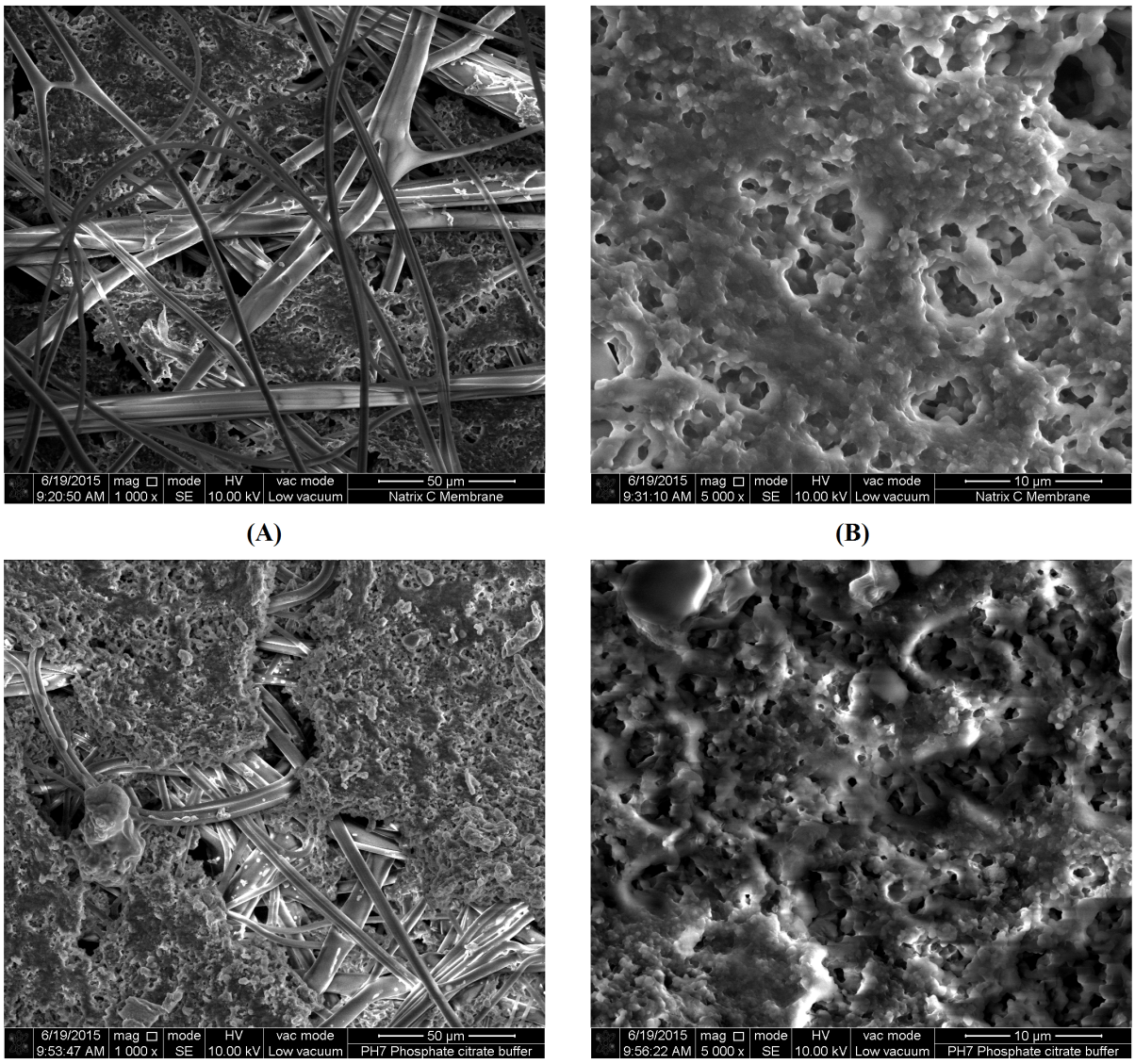

Figure 3-2 ESEM images of the surface of native dry Natrix C membrane with a magnification of (A) 1000 x and (B) 5000 x and surface of dried Natrix C membrane equilibrated in pH 7 phosphate citrate buffer and subsequently freeze-dried, with a magnification of (C) 1000 x and (D) 5000 x.

3.3.2 Effect of Buffer on Static Protein Adsorption

As membrane swelling and ESEM indicated significant effect of pH and moderate effect of ionic strength on swelling behavior, the effect of buffer on static protein adsorption for two different proteins, lysozyme and IgG, was evaluated from equilibrium binding characteristics, namely protein adsorption isotherms.

Protein adsorption with cation exchange membrane can be broadly perceived as the outcome of electrostatic interactions between negatively charged membrane and positively charged protein. However, at a molecular level, adsorption behavior is complex, where surface chemistry, pore size, and pore size distribution of membrane, protein amino acid composition, surface charge distribution and binding orientation should be taken into account [58]. By investigating and comparing the effect of ion content at constant pH on protein adsorption isotherm characteristics, some information on charge interaction was obtained. Protein adsorption at equilibrium was analyzed with the two-parameter Langmuir adsorption model and the five-parameter steric mass-action model.

3.3.2.1 Langmuir Model and Lysozyme

The adsorption isotherm profile of lysozyme on Natrix C membrane (Figure 3-3) exhibited nearly a rectangular shape as observed previously by Wang *et al.* [62] for lysozyme and Sartobind C and Sartobind S membrane in 10 mM potassium phosphate buffer at pH 7. Saturation adsorption occurred when equilibrium protein concentration reached 0.5 mg/mL in phosphate citrate buffer and 1 mg/mL in acetate buffer. Protein binding equilibrium adsorption (q_e) for lysozyme fitted well to the Langmuir adsorption model, with an R^2_{adj} of 0.988 in pH 5 phosphate citrate buffer and 0.960 in pH 5 acetate buffer.

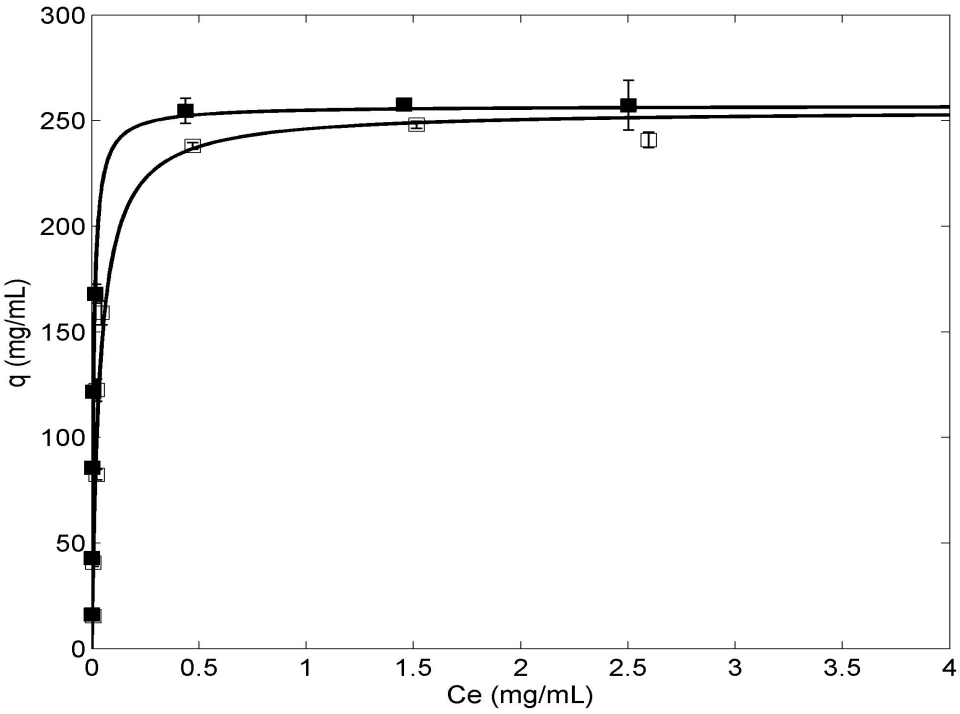

Figure 3-3 Adsorption isotherms for lysozyme and Natrix C membrane in (■) phosphate citrate buffer, and in (□) acetate buffer at pH 5 for 72h. The curves represent the estimates with the Langmuir model. Error bars represent standard error (n=3).

One of the assumptions of the Langmuir model requires that adsorbed molecules do not affect the availability of vacant binding sites, which occurs when the diameter of the adsorbed molecule is smaller than the average distance between adjacent sites. Lysozyme has a molecular weight of 14.3 kDa and a hydrodynamic radius of 2 nm [20]. It is possible that the relatively small size of lysozyme enables its adsorption isotherm to meet the assumptions of the Langmuir model.

Fitted parameters of the Langmuir model for lysozyme in phosphate citrate and acetate buffer are summarized in Table 3-4. When comparing q_{max} and K estimates, one has to keep in mind the quality of the experimental data and the changes captured by these two parameters, saturation level for q_{max} and change in slope for K. Previous work [70] reported smaller relative standard deviation for q_{max} estimates compared to K estimates obtained from protein binding data generated by Monte Carlo methods. For lysozyme, the maximum binding capacity q_{max} was similar for the two buffer types (257 mg/mL in

phosphate citrate buffer and 255 mg/mL in acetate buffer). The values of q_{max} in this work are significantly higher than most of the published literature (Table 3-5) values, while it is comparable with the q_{max} value for lysozyme with SP Sepharose XL resins (tentacle type) in sodium phosphate buffer at pH 7 with ionic strength of 19 mM.

The equilibrium constant K, reflecting the slope of the linear region of the adsorption isotherm, is an indicator of adsorption affinity. The K value in phosphate citrate buffer (121 mL/mg) was five times larger than for acetate buffer (27 mL/mg). K values for lysozyme and Natrix C membranes are comparable to those for Sartobind C and Sartobind S membranes and tentacle type resins [62, 71]. High K values illustrate the strong adsorption affinity between lysozyme and Natrix C membrane. Lysozyme (pI=11) has a strong positive charge at pH 5, dominating the electrostatic interaction with negatively charged carboxylic acid groups of Natrix C membrane, resulting in high adsorption affinity.

Table 3-4 Fitted Langmuir model parameters for lysozyme and IgG with Natrix C membrane.

Protein	Buffer type (pH 5)	q_{max} (mg/mL)	q_{max} (mmol/mL)	K (mL/mg)	K (mL/mmol)	R^2_{adj}
Lysozyme	Phosphate citrate	257	1.77×10^{-2}	121	1.76×10^{6}	0.988
	Acetate	255	1.76×10^{-2}	27.5	3.98×10^{5}	0.960
IgG	Phosphate citrate	119	7.93×10^{-4}	2.23	3.55×10^{5}	0.963
	Acetate	214	1.43×10^{-3}	0.96	1.44×10^{5}	0.973

Table 3-5 Published parameters of Langmuir model for lysozyme with cation exchange chromatography materials.

Material	Buffer	q_{max} (mg/mL)	K (mL/mg)	Reference
SP Sepharose FF (Strong cation)	100 mM sodium acetate; pH 5	120	52.63[a]	[44]
	10 mM sodium phosphate; pH 7; IS: 19 mM, 50 mM, 100 mM	82.9; 95.7; 113.3	14.7; 91.6; 100.8	[23]
SP Sepharose XL (Strong cation; Tentacle type)	10 mM sodium phosphate; pH 7; IS: 19 mM, 50 mM, 100 mM	147.4; 184.3; 203.5	11.8; 52.5; 3223.9	[23]
Sartobind S (Strong cation)	25 mM phosphate; pH 7	77.7± 6.1	8.3 ± 3.0	[71]
	10 mM potassium phosphate; pH 7	44	76	[62]
Sartobind C (Weak cation)	10 mM potassium phosphate; pH 7	23	62	[62]
Source 15S (Strong cation exchange polystyrene with SO_3^- ligands); EMD Fractogel SO_3 (Methacrylate; tentacle type)	6 mM sodium phosphate; pH 7	114; 178	166.9; 249.2	[22]
Poly (acrylic acid) modified regenerated cellulose membrane	10 mM potassium phosphate; pH 7	102.9	31.3[a]	[46]
P81 (Weak cation exchange membrane)	20 mM sodium phosphate; pH 7	46.52±17.83	3.57[a]	[72]
Poly (NASS)-modified RC membranes (24h SI-ATRP)	20 mM potassium phosphate; pH 7	138.3	1.918	[45]

[a] K (mL/mg) values were calculated from K_d (mg/mL)

The distinct K values according to buffer are indicative of the effect of buffer on protein adsorption by interacting with the protein and the adsorbing surface. Previous work [38] suggested that the valence of buffer ions could affect the global net surface charge of protein. Multi-valent counter-ions in buffer, such as HPO_4^{2-} and $C_6H_6O_7^{2-}$ in the phosphate citrate buffer, can bind to the protein surface and compensate the positive charge of lysozyme. With reduced lysozyme net surface charge, its adsorption affinity should be lowered which contradicts experimental observations where K value of lysozyme with Natrix C membrane in phosphate citrate buffer was higher than for the acetate buffer. It can be concluded that adsorption affinity of lysozyme on Natrix C could not be simply explained by its global net charge [58].

The charge distribution on a protein surface has also been identified to contribute to protein orientation during its adsorption as discussed by Dismer and Hubbuch [22] for lysozyme binding on two different cation exchange resins. Lysozyme orientation may be changed by the ion composition of buffer, which could explain the differences in K values according to buffer for lysozyme binding with Natrix C membranes. The macroporous hydrogel layer could act like a tentacle type resin and induce protein reorientation. Therefore, it is postulated that phosphate citrate buffer facilitates the local charged region of lysozyme for binding. Further investigations on this point will be needed and could be achieved by labeling of lysine residue of the protein as described by Dismer and Hubbuch [22].

In addition to ionic interactions, hydrophobic interactions may also contribute to the adsorption process of ion exchange chromatography. Hydrophobic interactions involve an initial step, dehydration and deionization of the protein surface [73]. Buffers with solute of higher molar surface tension can facilitate the expulsion of the protein from the solvent, therefore facilitating the adsorption process [74]. The molar surface tension of phosphoric acid (74.6 mN/m) is higher than for acetic acid (27.4 mN/m) [75]. It is proposed that phosphate citrate buffer may facilitate the initial water replacement step for lysozyme and Natrix C, thus a higher K value was achieved.

3.3.2.2 Langmuir Model and IgG

Protein adsorption behavior is also affected by protein size and surface charge characteristics. The effect of these properties was investigated by conducting adsorption isotherms for IgG, a significantly larger protein with molecular weight of 150 kDa, and hydrodynamic radius of 5.4 nm and different isoelectric point properties than lysozyme. IgG has 77% of its constituents with pI above pH 8 giving a net positive charge at pH 5 [33]. Adsorption isotherm profiles for IgG (Figure 3-4) was distinct from that of lysozyme (Figure 3-3), reflected by the smaller slope of the linear portion and lower maximum adsorption capacity. The saturation point for IgG was observed at a higher equilibrium protein concentration than for

lysozyme. In phosphate citrate buffer, the saturation was reached at 2 mg/mL while it hasn't reached until 4 mg/mL in acetate buffer.

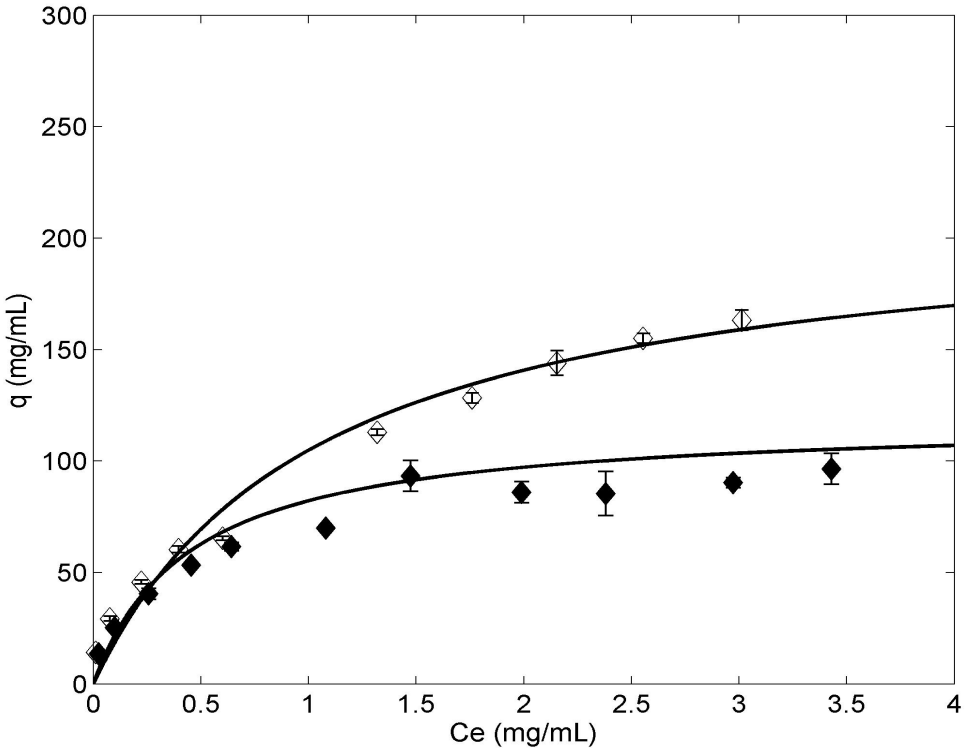

Figure 3-4 Adsorption isotherms for IgG and Natrix C membrane in (◆) phosphate citrate buffer, and in (◊) acetate buffer at pH 5 for 24h. The curves represent the estimates with the Langmuir model. Error bars represent standard error (n=3).

Representation of the experimental IgG isotherm with the Langmuir model was relatively similar to that of lysozyme, with an average R^2_{adj} value of 0.963 in phosphate citrate buffer and 0.973 in acetate buffer. The estimated maximum binding capacity (Table 3-4) was 119 mg/mL in phosphate citrate buffer and 214 mg/mL in acetate buffer, of the same magnitude as reported by Müller-Späth *et al.* [76] for the saturation capacity (120mg/mL) of IgG with strong cation resin Fractogel SO_3 (M) in 20 mM phosphate at pH 6. The estimated equilibrium constant in this work was at least two orders of magnitude higher than the published values from Wrzosek *et al.* [77], where K_d ($K=1/K_d$) was reported as 140 ± 35 mg/mL for IgG with strong cation resin FractoGel EMD SE Hicap (M) in 50 mM phosphate citrate buffer at pH 4.5.

Estimated Langmuir parameters for IgG were significantly different in the two buffer types. The maximum binding capacity q_{max} was 80% higher in acetate buffer than phosphate citrate buffer; while the equilibrium constant K was 130% higher in phosphate citrate buffer than acetate buffer. With the complex characteristics of IgG, the competitive binding with salts and adsorption affinity towards the membrane may be greatly changed by variations of the buffer content [32]. Therefore, the differences in the adsorption behavior for IgG may be due to the difference in salt counter-ion (Na^+) concentration of the buffer. The concentration of Na^+ is 47% higher in phosphate citrate buffer (206 mmol/L) than acetate buffer (140 mmol/L), corresponding to the difference in the maximum binding capacity. A previous study [59] reported decreasing static binding capacity with increasing ionic strength at pH 5 with IgG and polymethacrylate based cation exchange membranes (sulfoisobutyl ligand groups) in 50 mM phosphate citrate buffer.

3.3.2.3 Langmuir Model and Effect of Protein Type

Estimated Langmuir model parameters for lysozyme and IgG were compared on a mass basis and molar basis. The maximum binding capacity for the two proteins is comparable on mass basis, which when compared on a molar basis are quite different and reflect the differences in molecular weight of IgG which is nearly 10 times larger than lysozyme. The molar q_{max} value for lysozyme is 23 times and 13 times larger than the molar q_{max} value for IgG in phosphate citrate buffer and in acetate buffer, respectively. The significant difference is partially explained by the difference in the protein molecules size. Tatárová *et al.* [71] reported decreasing dynamic binding capacity (DBC) values with protein molecule size, where $DBC_{10\%}$ was determined for bovine serum albumin (M_w=66.4 kDa), β-lactoglobulin (M_w=18.4 kDa), myoglobin (M_w=16.7 kDa), and lysozyme (M_w=14.4 kDa) as 17.8 mg/mL, 25.4 mg/mL, 30.4 mg/mL, and 34.5 mg/mL with Sartobind S. Protein with large size may shield significant number of salt counter-ions on the membrane surface upon adsorption that would otherwise be available for exchange with the protein molecules in the mobile phase. The binding orientation of IgG may also contribute to its adsorption behavior, which could be magnified because of its size. Higher accessibility to active binding sites for protein molecules with smaller size was observed with confocal laser scanning microscopy [78], which could contribute to the higher maximum binding capacity with lysozyme.

The equilibrium constant (K) of the two proteins were comparable on a molar basis while the K value for lysozyme was higher than IgG on a mass basis, which may result from the difference of the percentage of basic surface residues on lysozyme and IgG. Lysine and arginine are positively charged amino acid residues, which will be completely protonated at pH 5, while histidine residues will be

partially protonated for its lower pK_a. Lysozyme and IgG have similar percentage of lysine residues, 4.7% for lysozyme [23] and 6.2% for IgG [30]. However, lysozyme has a significantly higher percentage of arginine residues (8.5%) than IgG (3.7%), which means that its surface charge density is higher than IgG. Therefore, the adsorption affinity induced by electrostatic interactions is stronger for lysozyme, which could explain its higher equilibrium constant. In addition, the large size of IgG may lead to stronger mass transport limitations and thus slower adsorption rate.

As the most commonly used protein adsorption equilibrium model, the model was found appropriate in describing the adsorption of lysozyme and IgG to Natrix C membrane in the present work, with a satisfactory R^2 value at low ionic strength. For different protein type, the estimated parameters for the Langmuir model, q_{max} and K, are mainly dependent on the protein size and percentage of basic (acidic) surface residues. With smaller size and stronger positive charges, lysozyme achieved higher binding capacity and stronger adsorption affinity. Therefore the adsorption of lysozyme was dominated by protein charge and the buffer effect was negligible. For IgG with moderate protein charge, however, the buffer effect was significant and will be discussed further in the following section.

3.3.2.4 Langmuir Model and Effect of Salt

The primary influence on protein adsorption by ion exchange is the salt counter-ions in the buffer that are involved in the competitive binding with the protein molecules and cause shielding of the protein charge. Buffers with distinct ion content (ion valence) may have great influence on the global net surface charge, charge distribution, and the spatial binding orientation of protein molecules. Other minor effect of salt may be facilitating the “water replacement” process in hydrophobic interactions. Buffers also have a significant effect on the structure of hydrogel containing adsorption systems. For example, the ionic strength of the buffer determines the availability of active binding sites in the membrane for hydrogel containing membranes.

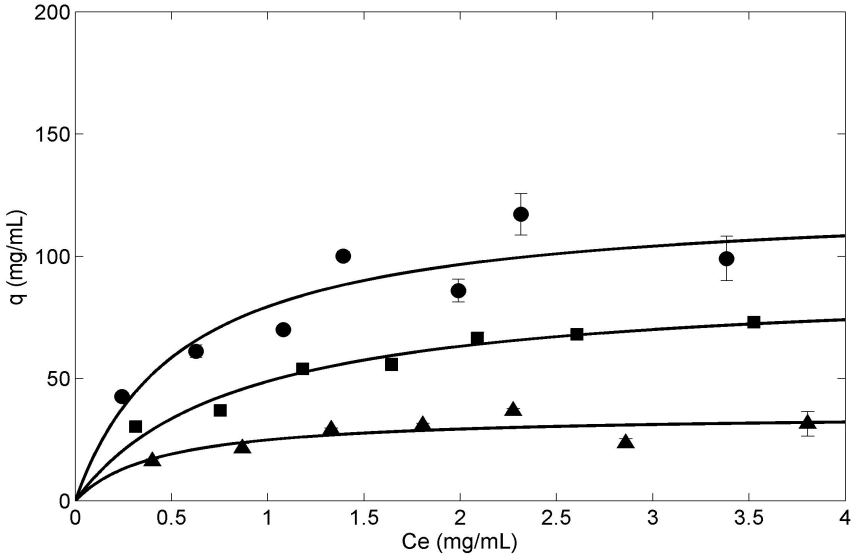

(A)

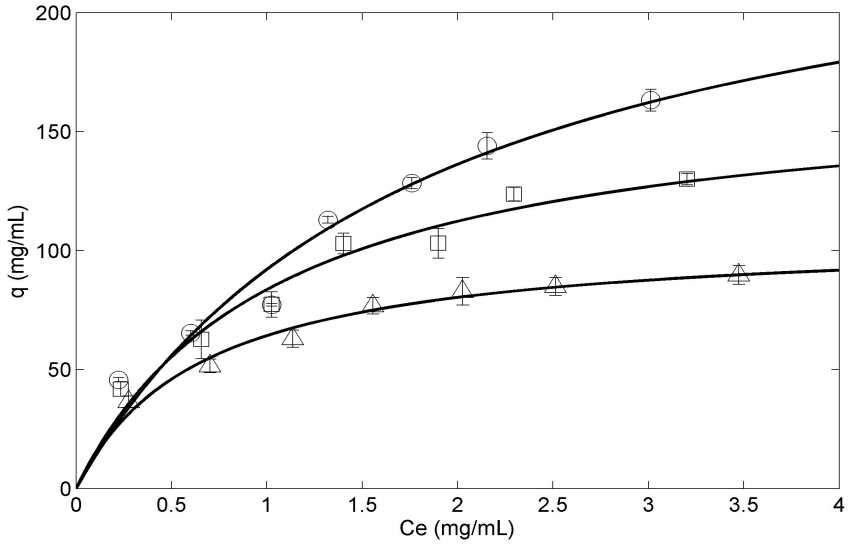

(B)

Figure 3-5 Adsorption isotherms for IgG and Natrix C membrane in (A) phosphate citrate buffer with ionic strength of (●) 206 mM; (■) 256 mM; (▲) 306 mM at pH 5 and in (B) acetate buffer with ionic strength of (O) 140; (□) 190 mM; (Δ) 240 mM at pH 5. The curves represent the estimates with the Langmuir model. Error bars represent standard error (n=3).

The effect of the salt counter-ion concentration of buffers on protein adsorption was investigated by adding 50 mM and 100 mM NaCl in pH 5 phosphate citrate buffer and pH 5 acetate buffer. The protein binding equilibrium adsorption (q_e) in phosphate citrate buffer and in acetate buffer with increased ionic strength was fitted into the Langmuir adsorption model for IgG (Figure 3-5). The isotherm profiles exhibited decreasing maximum binding capacity with increasing buffer ionic strength. Saturation point was reached at lower protein concentration with higher ionic strength. Representations of the experimental IgG isotherm in phosphate citrate buffer with the Langmuir model was satisfactory until ionic strength reached 306 mM, where the R^2 was only 0.478, while the representations for the isotherm in acetate buffer was very good for all ionic strength considered.

The parameters of the Langmuir model, estimated for each ionic strength condition of the phosphate citrate buffer and acetate buffer, are summarized in Table 3-6. The maximum binding capacity q_{max} (Figure 3-6) and the equilibrium constant K (Figure 3-7) for the two buffers were combined and plotted against buffer ionic strength, C_s. q_{max} decreased with ionic strength and exhibited a linear relationship with R^2=0.95. The pronounced effect of buffer ionic strength on q_{max} was also reported by Dismer *et al.* [23], where the maximum binding capacity for lysozyme decreased 13% with SP Sepharose FF and 20% with SP Sepharose XL, when ionic strength of sodium phosphate buffer increased from 50 mM to 100 mM.

Table 3-6 Fitted Langmuir model parameters for IgG and Natrix C membrane in buffers at pH 5 with increased ionic strength.

Buffer	C_s (mM)	q_{max} (mg/mL)	K (mL/mg)	R^2
Phosphate citrate	206	123	1.8	0.725
	256	89	1.2	0.906
	306	36	2.3	0.478
Acetate	140	262	0.54	0.935
	190	171	0.96	0.889
	240	107	1.50	0.890

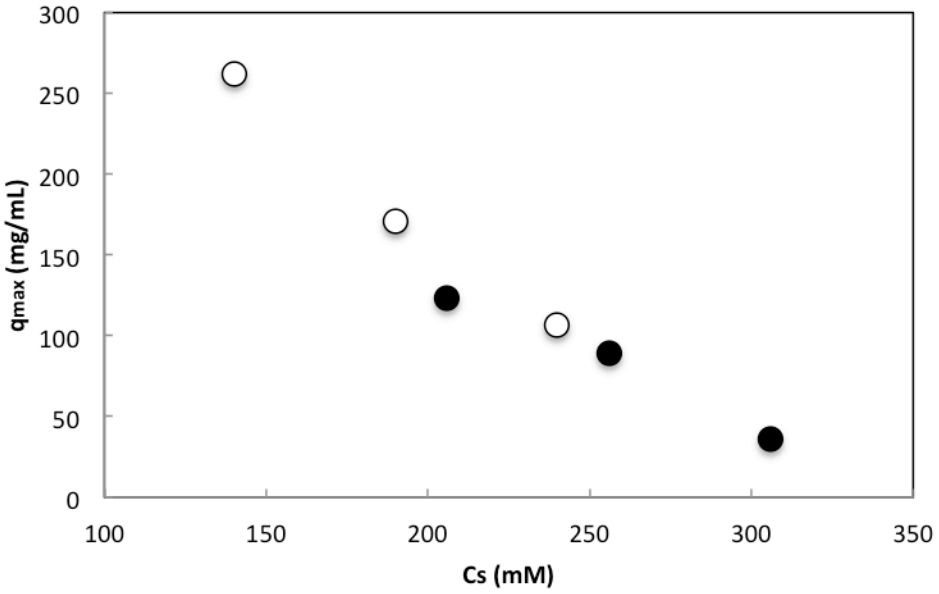

Figure 3-6 Maximum binding capacity as a function of salt concentration for (●) phosphate citrate buffer and (○) acetate buffer.

Buffer ionic strength may influence the protein adsorption process by altering the pore size of the membrane, thus altering the availability of binding sites on the pore surface. Hassel [16] reported significant effect of KCl addition on reducing the fraction of pores larger than 0.96 μm at pH 6 and pH 7 for Natrix C. Tatárová *et al.* [61] observed that the volume of the gel layer decreased from 35% of total pore volume to 20% with an increase of ionic strength from 0M to 1M for a strong anion exchange membrane Sartobind Q. The membrane is formed by macroporous cellulose support and a hydrogel layer at the pore surface. Effect of buffer ionic strength on the pore size was also reported for tentacle type resins, *i.e.* cation exchange resins Fractogel SO_3 (M) [76]. It was suggested that the tentacle structure in the resin pores is sensitive to buffer ionic strength, since high salt concentration may suppress tentacle charges and shrink pores that induce larger mass transfer limitations.

Buffer ionic strength also plays an important role in the adsorption behavior of protein through competitive binding. With increased Na^+ concentration, there exists fierce competition between the salt counter-ions and protein molecules for binding sites on the membrane surface. The smaller size of salt ions is favorable for penetrating the pores and adsorbed on the binding sites, compared with macromolecules like IgG. Therefore, the binding capacity decreased significantly for IgG when the ionic strength increased from 256 mM to 306 mM for phosphate citrate buffer.

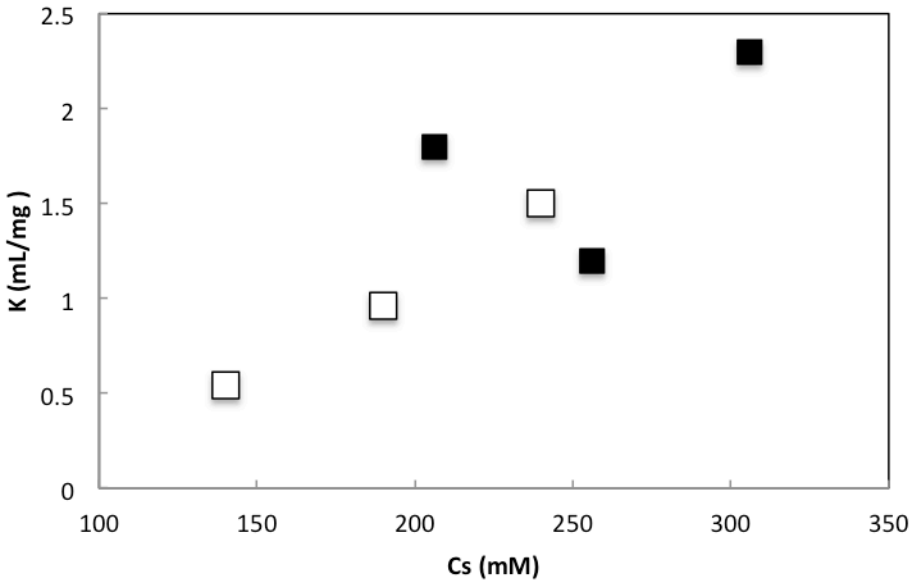

Figure 3-7 Equilibrium constant as a function of salt concentration for (■) phosphate citrate buffer and (□) acetate buffer.

The estimated equilibrium constant K for IgG with Natrix C membrane increased with increasing ionic strength for acetate buffer, while no trend was observed for phosphate citrate buffer. It contradicts with the theory proposed in the literature that K decreases with ionic strength. Dismer *et al.* [23] suggested that higher ionic strength will decrease the adsorption affinity between lysozyme and the adsorbent, leading to dissociation of the protein molecules. In this work, however, the structure and properties of IgG are more complex than lysozyme. Moreover, the distinct morphology of Natrix C membrane used may also lead to variations in the adsorption isotherm.

In addition to its influence on binding capacity and equilibrium constant, the buffer ionic strength may also have an impact on the binding orientation of adsorbed protein molecules. Dismer *et al.* [23] observed

that the labeling efficiency of lys116 increased 7% when the ionic strength of sodium phosphate buffer (pH 7) increased from 19 mM to 50 mM. They proposed that it was due to the tilt of adsorbed lysozyme molecules on SP Sepharose FF at higher ionic strength. The ionic strength of buffer may also induce pH decrease of the mobile phase [63]. The magnitude and duration of pH decrease are dependent on the buffer type, where the pH decreased 0.1 units, 0.15 units, and 0.3 units in acetate buffer, citrate buffer and phosphate citrate buffer, respectively.

By investigating the protein adsorption of IgG with Natrix C membrane in phosphate citrate buffer and acetate buffer with different ionic strength, the salt counter-ion concentration was found to have a significant impact on the estimated Langmuir parameters. The maximum binding capacity decreased linearly with ionic strength, probably due to reduced accessibility of binding sites and competitive binding. The increasing equilibrium constant with ionic strength, which contradicted with the literature for lysozyme, may be explained by the complex surface characteristics of IgG and distinct structure of Natrix C membrane. The ionic strength of buffer was also reported having influence on the binding orientation of protein and pH transition during the binding process.

3.3.2.5 Steric Mass-action Model

In order to gain a more comprehensive understanding of the adsorption process, the steric mass action (SMA) model was employed in the following work, where multi-point binding and salt effect were taken into account [49]. The protein equilibrium adsorption (q_e) of IgG with Natrix C membrane in pH 5 phosphate citrate buffer (Figure 3-8) and pH 5 acetate buffer (Figure 3-9) for three different NaCl concentration was fitted with the SMA model. The isotherm profiles showed that the SMA model successfully predicted the decreasing binding capacity and decreasing initial slope with increased buffer ionic strength. The SMA equilibrium parameters were assumed to be constant and independent of protein and salt concentration [49]. Nevertheless, the model estimates of the equilibrium protein binding capacity for IgG was lower than the corresponding experimental results at low protein concentration, while higher estimates were obtained at high protein concentration. The deviation of the model predictions may be that the SMA model represents only adsorption and does not account for the mass transport during the ion exchange process. Mass transport limitations can become significant factors affecting adsorption behaviors of macromolecules that possess large size, *e.g.* IgG.

The SMA model gave a better representation of the protein adsorption in acetate buffer (R^2=0.822) than for phosphate citrate buffer (R^2=0.490). The quality of the experimental data for the phosphate citrate buffer and IgG equilibrium concentration higher than 1mg/ml could also explain the differences. It is thus

proposed that the buffer type and buffer conditions have an influence on the adsorption of IgG with the Natrix C membrane.

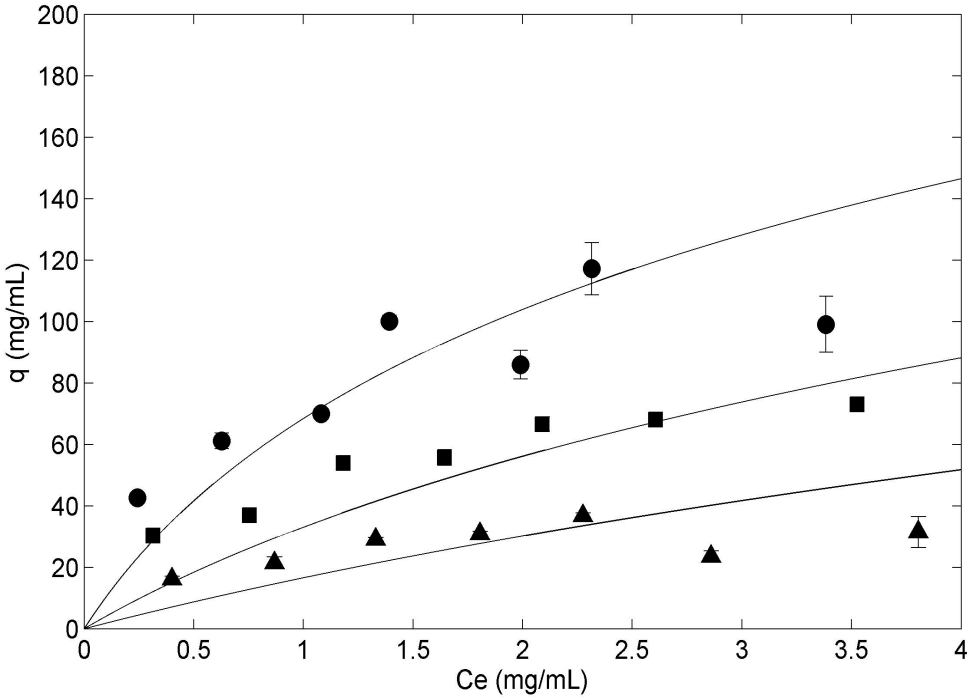

Figure 3-8 Adsorption isotherms of IgG in pH 5 phosphate citrate buffer with different sodium ion concentration C_s (●) 206 mM; (■) 256 mM; (▲) 306 mM. The curves represent the estimates with the SMA model. Error bars represent standard error (n=3).

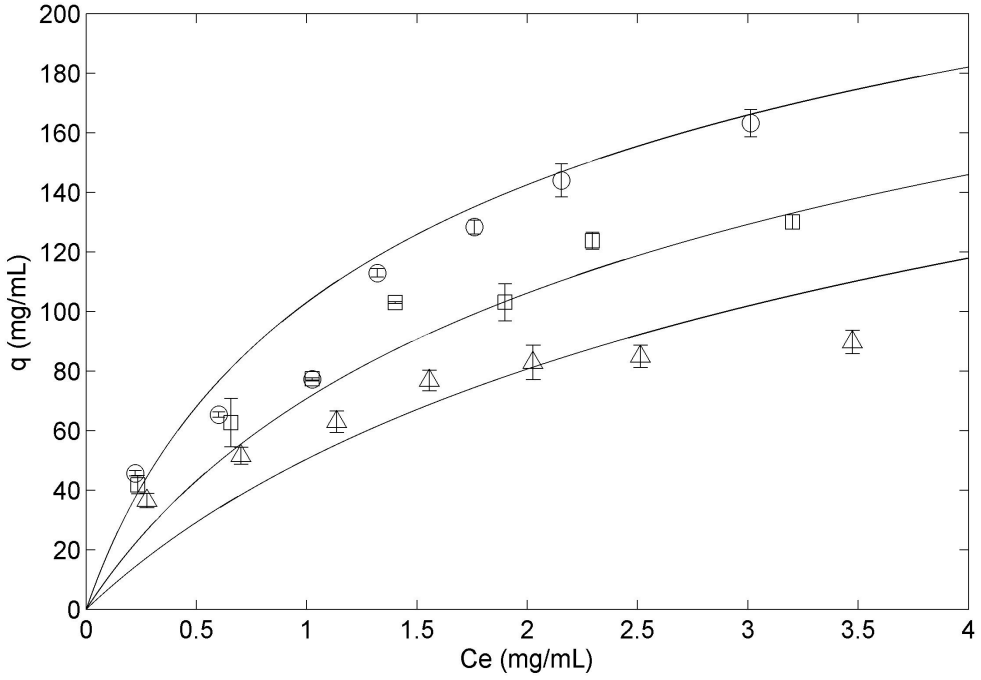

Figure 3-9 Adsorption isotherms of IgG in pH 5 acetate buffer with different sodium ion concentration C_s (○) 140 mM; (□) 190 mM; (Δ) 240 mM. The curves represent the estimates with the SMA model. Error bars represent standard error (n=3).

The physical interpretation of the SMA parameters is essential for understanding the adsorption process. The equilibrium constant (K_a), given as the ratio of the protein adsorption and desorption coefficients, describes the adsorption affinity between the protein and the adsorbent. The characteristic charge (ν), the number of charged sites on the protein that actually interacts with the ion exchanger upon adsorption displacing an equivalent amount of monovalent salt counter-ions, accounts for the multipoint binding of the protein. The steric hindrance effect is represented by the steric factor (σ), which stands for the number of sites on the adsorbent surface shielded by the protein and thus prevented from exchanging with proteins in the mobile phase. The ion exchange capacity (A) of the membrane was assumed to be constant during the adsorption process, and was measured previously as 204 mM. The mobile phase salt concentration (C_s) was taken as the experimental counter-ion (Na^+) concentration.

The fitted parameters of the SMA model for IgG with the two buffer types are summarized in Table 3-7. The characteristic charge (ν) was determined as 4.52 in phosphate citrate buffer and 2.08 in acetate buffer respectively, which indicates that approximately two additional charged sites on each protein

molecule are bound to the membrane in phosphate citrate buffer. The equilibrium constant (K_a) was estimated to be 18% higher in phosphate citrate buffer than in acetate buffer. The steric factor (σ) in phosphate citrate buffer was half the one estimated for acetate buffer. There are no estimated SMA parameters available in the literature for IgG with cation exchange membrane or resin.

Previous work reported higher mean relative deviations (0.5%) for the steric factor and the equilibrium constant than the characteristic charge (0.25%) [57]. The value of the standard deviation corresponds with the physical meaning of the parameters. Characteristic charge is relatively stable for a fixed protein-adsorbent system. The equilibrium constant represents the rate of the adsorption process, which may be susceptible to various factors. Therefore when analyzing the estimated parameters, more emphasis will be laid on the effect of buffer on characteristic charge.

Table 3-7 Fitted SMA model parameters for IgG and Natrix C membrane in two buffers at pH 5.

Buffer type at pH 5	ν	K_a	σ
Phosphate citrate	4.52	115	41.0
Acetate	2.08	97.8	86.3

The estimated characteristic charge ν is predetermined by buffer pH and isoelectric point (pI) of protein, while independent of buffer ionic strength. van Beijeren *et al.* [79] reported that the estimated ν increased from 3.85 to 7.07 when buffer pH increased from 5.3 to 7.0 for BSA (pI=4.7) with Sartobind Q. Due to the asymmetrical distribution of charge on the protein surface, the estimated ν can be significantly different from the net surface charge of protein at a corresponding pH. Since the phosphate citrate buffer and acetate buffer used in this work were at the same pH 5, it is postulated that the differences between the estimated characteristic charge in the two buffers result from the valence of ions. The adsorption of multivalent anions like phosphate and citrate onto the protein surface may affect the zeta potential of positively charged protein, and therefore affect its surface charge distribution. The SMA model assumes a single charge state or a constant characteristic charge of the adsorbed protein during the whole adsorption process. However, the electrostatic field of the membrane surface may affect the net charge on the protein. In order to incorporate the "charge regulation" phenomenon, Shen and Frey [55] extended the traditional SMA model and developed a multiple charge state model.

The equilibrium constant determines the adsorption affinity between the protein and the membrane. Shi *et al.* [64] conducted the finite batch experiment and observed that the estimated value of K_a for BSA with

DEAE Sepharose FF decreased with increasing ionic strength. It was proposed that the effect of ionic strength on the binding of IgG on Natrix C membrane was due to competitive binding of salt counter-ions that suppressed the electrostatic interactions between the protein and the membrane. In this work, the salt concentration of phosphate citrate buffer was twice that of acetate buffer, while the K_a determined for phosphate citrate buffer was 18% higher than for acetate buffer. This could be explained by the effect of multivalent anions in phosphate citrate buffer. Harinarayan *et al.* [39] suggested an exclusion mechanism, indicating that proteins in the mobile phase are impeded from interacting with the binding sites on the membrane by charge repulsion with the adsorbed proteins. The multivalent anions in phosphate citrate buffer may specifically adsorb onto the surface of protein molecules, compensating the positive charges. This may alleviate the charge repulsion between proteins and result in higher adsorption affinity.

The smaller estimated steric factor in phosphate citrate buffer suggests reduced hindrance of the binding sites on the membrane by the adsorbed protein than in acetate buffer. van Beijeren *et al.* [79] reported that the value of steric factor decreased with increasing ionic strength and proposed that it was due to more compact conformation of adsorbed protein. Dzhafarov [80] reported increased surface area accessibility of bovine serum albumin (BSA) during the structural transformation from heart-shape (N form) to cigar-shape (F form) at decreasing pH.

3.3.2.6 SMA Model Parameter Sensitivity Analysis

SMA model parameter sensitivity analysis was conducted for protein adsorption of IgG with Natrix C membrane in phosphate citrate buffer at pH 5. Each parameter was varied by ±20% based on the previously estimated values (ν= 4.52, σ= 41.0 and K_a = 115) while keeping the other two parameters constant. Adsorption isotherms were generated for conditions at low salt concentration (206 mM) and high salt concentration (306 mM).

By considering two domains, protein concentration near zero and saturation conditions, one can further investigate the contribution of each SMA parameter. For linear conditions where protein concentration approaches zero, the adsorption isotherm (Equation 2-21) is simplified as,

$$\lim_{C \to 0} q_e = K_a \left(\frac{\Lambda}{C_s}\right)^{\nu} C \qquad \textbf{Equation 3-16}$$

The initial slope of the isotherm is denoted by the term $K_a \left(\frac{\Lambda}{C_s}\right)^{\nu}$. Therefore the slope is determined by the equilibrium constant (K_a) and the characteristic charge (ν).

For overloaded conditions where saturation is reached, the maximum binding capacity given by the SMA model is determined by the characteristic charge and the steric factor. The steric factor is the non-linear parameter, accounting for the nonlinear adsorption effects.

$$\lim_{C \to \infty} q_e = \frac{\Lambda}{\sigma+\nu} = q^{max} \qquad \textbf{Equation 3-17}$$

Estimated adsorption isotherms revealed that the protein binding estimates were most sensitive to the characteristic charge, especially the initial non-linear part of the adsorption isotherm (Figure 3-10 A). The high sensitivity to the characteristic charge may be explained by its position as an exponent in the model equation (Equation 3-16). The estimated binding capacity decreased with increasing ν, since the ion exchange capacity of the membrane is finite [49] and increased ν will reduce the number of available binding sites for protein adsorption. The equilibrium constant K_a also had a significant effect on estimated protein binding, especially at low salt concentration.

The SMA model protein binding estimates were less sensitive to the steric factor σ, where the estimated adsorption isotherm remained nearly unchanged with varied σ at high salt concentration. It may be explained by the format of Equation 3-17, where σ exists as part of the denominator. Similar to the characteristic charge, the steric factor also showed influence on the non-linear region of adsorption isotherm. The binding capacity decreased with increasing σ due to reduced available binding sites.

The sensitivity analysis revealed that all three parameters influenced the SMA model protein adsorption estimates, with ν the most significant while σ the least. Since ν, K_a, and σ were determined simultaneously based on one equation (Equation 3-6), it would be of interest to further investigate the sensitivity of SMA parameter estimations to each other to understand their correlations. Osberghaus *et al.* [57] conducted a sensitivity analysis for SMA parameters and observed high sensitivity of estimated K_a towards changes in ν, where the estimated K_a decreased significantly with fixed ν value. Literature has also suggested correlating the salt concentration with one of the SMA parameters for better predictability of the SMA model under various buffer conditions [56, 64].

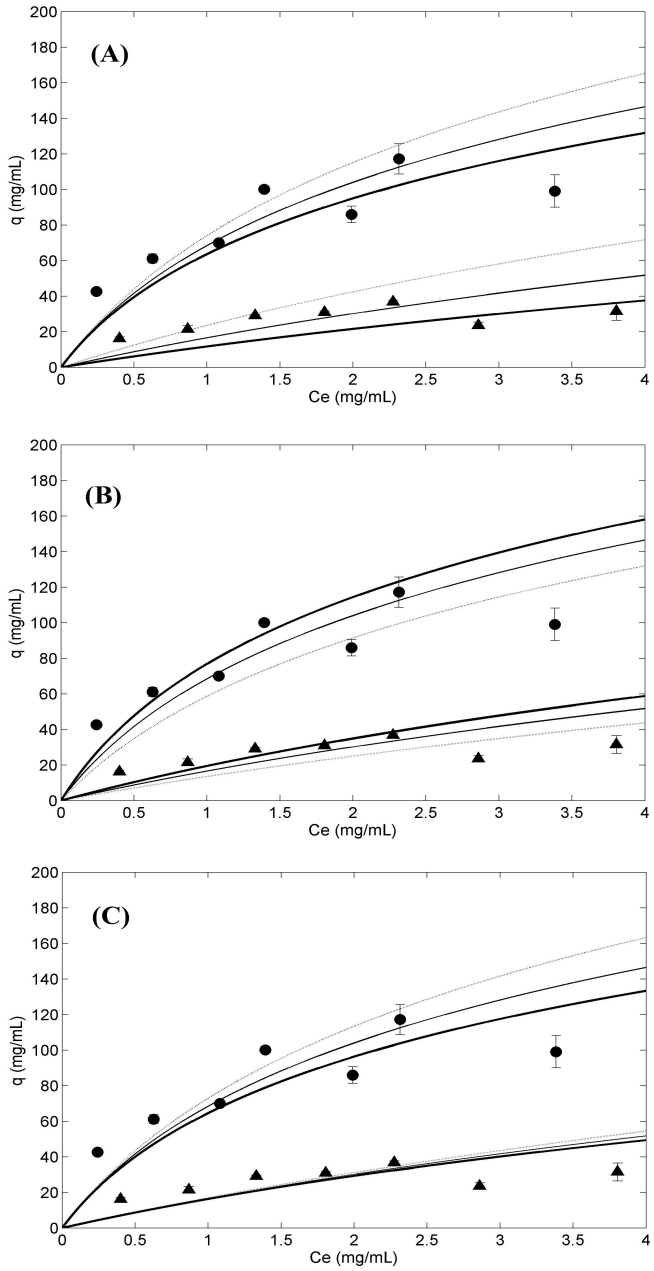

Figure 3-10 Adsorption isotherms of IgG in pH 5 phosphate citrate buffer with salt counter-ion concentration C_s (●) 206 mM and (▲) 306 mM. The curves represent the estimates with the SMA model with varied parameters (A) v: 4.52±20%, (B) K_a: 115±20%, and (C) σ: 41±20%, where the value of the parameters are represent by the width of the lines. Error bars represent standard error (n=3).

3.3.2.7 Comparison of SMA Model Estimates

The applicability of the SMA model in predicting protein adsorption isotherm for various proteins, *e.g.* lysozyme (Table 3-8) and bovine serum albumin (BSA) (Table 3-9) has been reported in a number of publications. With a molecular weight of ~14kDa and a pI of 11, the characteristic charge of lysozyme was determined to range from 4.07 to 7.12 and the steric factor ranged from 9.5 to 37, while the equilibrium constant spanned three orders of magnitude and was less than unity. Comparing the estimations from Osberghaus *et al.* [57] and Ladiwala *et al.* [54] , even with the same cation exchanger, same buffer type and pH, the deviation for the estimated SMA parameters were 19% for υ, 83% for K_a, and 54% for σ when buffer concentration increased from 20 mM to 50 mM. Different experimental approaches and estimation methods may also lead to deviations between estimated parameters [57]. Osberghaus *et al.* compared two approaches for determining the SMA parameters. One approach was based on gradient and frontal experiments, and the SMA parameters estimated for lysozyme with SP Sepharose FF in 20 mM acetate buffer pH 5 was $\nu = 4.72$, $K_a = 0.44$, and $\sigma = 36.8$. The second approach based on an inverse method and a mechanistic model, gave SMA parameters estimates as $\nu = 5.07$, $K_a = 0.12$, and $\sigma = 31.2$ for similar experimental conditions. Therefore, when evaluating the predictability of SMA model for protein adsorption isotherm, it is essential to identify the optimal operation condition, properties of ion exchanger and parameter estimation approach.

BSA is a common model protein in anion exchange chromatography, having a molecular weight of 66kDa and a pI of 5.4 [64]. The effect of buffer condition [64, 79] and charge regulation [55] on steric mass-action equilibrium has been evaluated with BSA. The investigations with BSA gave insights into the effect of buffer on IgG with cation exchange membrane in this work.

Table 3-8 Published SMA parameters for lysozyme with cation exchange chromatography materials.

Material	Buffer	υ	K_a	σ	Reference
SP Sepharose FF (Strong cation exchange resin)	20 mM sodium acetate; pH 5	4.72	0.441	36.8	[57]
	20 mM sodium phosphate; pH 7	4.07	0.17	29.74	[57]
	50 mM sodium acetate; pH 5	5.6	0.0763	17	[54]
Millipore strong cation exchange resin	100 mM sodium phosphate; pH 7.5	5.3	0.0148	34	[81]
	50 mM sodium phosphate; pH 6	5.95	0.0124	9.5	[53]
Source 15S (Strong cation exchange resin)	30 mM sodium phosphate; pH 6	5.5	1.1	14	[82]
Sartobind S75 (Strong cation exchange membrane)	25 mM acetate; pH 4.5	7.12	0.0049	-	[79]

Table 3-9 Published SMA parameters for bovine serum albumin (BSA) with anion exchange chromatography materials.

Material	Buffer	υ	K_a	σ	Reference
Sartobind Q75 (Strong anion exchange membrane)	25 mM acetate; pH 5.3; pH 7.0	3.85; 7.07	0.071; 0.512	-	[79]
DEAE Sepharose FF (Anion exchange resin)	20 mM acetate; pH 5	5.1	0.1	100	[55]
	20 mM acetate; pH 4.5-6.5	0.9-3.3	-	31	[64]

3.3.3 Effect of Buffer on Dynamic Protein Adsorption

Static protein adsorption exhibited significant effect of ion content and ionic strength of buffer on protein adsorption isotherms for lysozyme and IgG with Natrix C membranes. In order to further investigate the effect of buffer during protein adsorption with the Natrix C membranes, dynamic protein binding experiments were conducted. Protein binding in a dynamic mode allows for the minimization of mass transfer limitations by convection. The drawback is that the binding takes place under dynamic conditions, which results in lower binding than those under equilibrium conditions. By analyzing the shape of the breakthrough curve, information on internal mass transfer limitations can be obtained. Efficiency of protein binding can be obtained from dynamic binding capacity estimates at 10% breakthrough ($DBC_{10\%}$).

The effect of binding buffer pH, type of buffer and feed protein concentration on protein binding with the Natrix C membrane was investigated. The breakthrough curves of lysozyme with Natrix C membrane with various buffer conditions are given in Figure 3-11, where normalized absorbance denotes the ratio of the current detected absorbance over the absorbance of the feed and normalized time denotes the ratio of the current time over the total binding time. Figure 3-11 (A) compares the effect of pH on breakthrough curves for lysozyme with phosphate citrate buffer at pH 4.8 and pH 5, and feed lysozyme concentration of 0.5 mg/mL. The two breakthrough curves are similar in shape and slope, while an earlier 10% breakthrough point took place for buffer pH 4.8. Neither of the curves reached a plateau in the end, which means that the membrane was not fully saturated by the end of the binding cycle.

Figure 3-11 (B) compares the effect of feed lysozyme concentration (0.5 mg/mL and 2 mg/mL) with phosphate citrate buffer at pH 5. Different shapes of the breakthrough curves were observed for the two feed concentrations. For the 2 mg/ml lysozyme feed concentration, a sigmoidal shape was observed as reported in the literature. Gebauer *et al.* [83] obtained breakthrough curves for lysozyme with two types of Sartobind S membrane, exhibiting sigmoidal shape for all three protein concentration investigated, 0.1 mg/mL, 2 mg/mL, and 8 mg/mL. However, the breakthrough curve for the feed lysozyme concentration of 0.5 mg/ml in this study showed a distinct broad shape. Steeper slope and an earlier breakthrough point were observed at high protein concentration, indicating less mass transport limitations. Other than the convective transport of proteins in the membrane pores, there also exists diffusion of proteins in the hydrogel layers. Difference in the chemical potentials, *i.e.* protein concentration, is the driving force of protein diffusion [79]. Therefore, higher protein concentration may result in better mass transport efficiency.

The effect of buffer type on breakthrough curves is compared in Figure 3-11 (C), for lysozyme at pH 5 and 0.5 mg/mL feed concentration and phosphate citrate buffer and acetate buffer. Acetate buffer showed an earlier breakthrough point and steeper slope, indicating less mass transport resistances during dynamic binding than phosphate citrate buffer.

Breakthrough curves for different protein types, lysozyme and IgG, were compared with Natrix C, where binding buffer were acetate buffer at pH 5 with feed protein concentration at 0.5 mg/mL. (Figure 3-12) The two breakthrough curves were similar in shape, while earlier breakthrough was observed for lysozyme. Dynamic binding with lysozyme may present less mass transport limitations than IgG for its smaller size.

For ideal adsorbents without mass transport limitations, the shape of the breakthrough curves should be rectangular. Membranes are generally regarded as ideal adsorbents, compared to resins. However, the breakthrough curves obtained in the present work showed breakthrough curves of various shape and slope according to buffer conditions, indicating the existence of mass transport limitations. Further analysis of the mass transport during dynamic binding of proteins with the Natrix C could be achieved by establishing mathematical models as previously reported [84-86]. However, this work would require knowledge of the membrane porosity, and axial dispersion coefficient that are beyond the scope of this thesis.

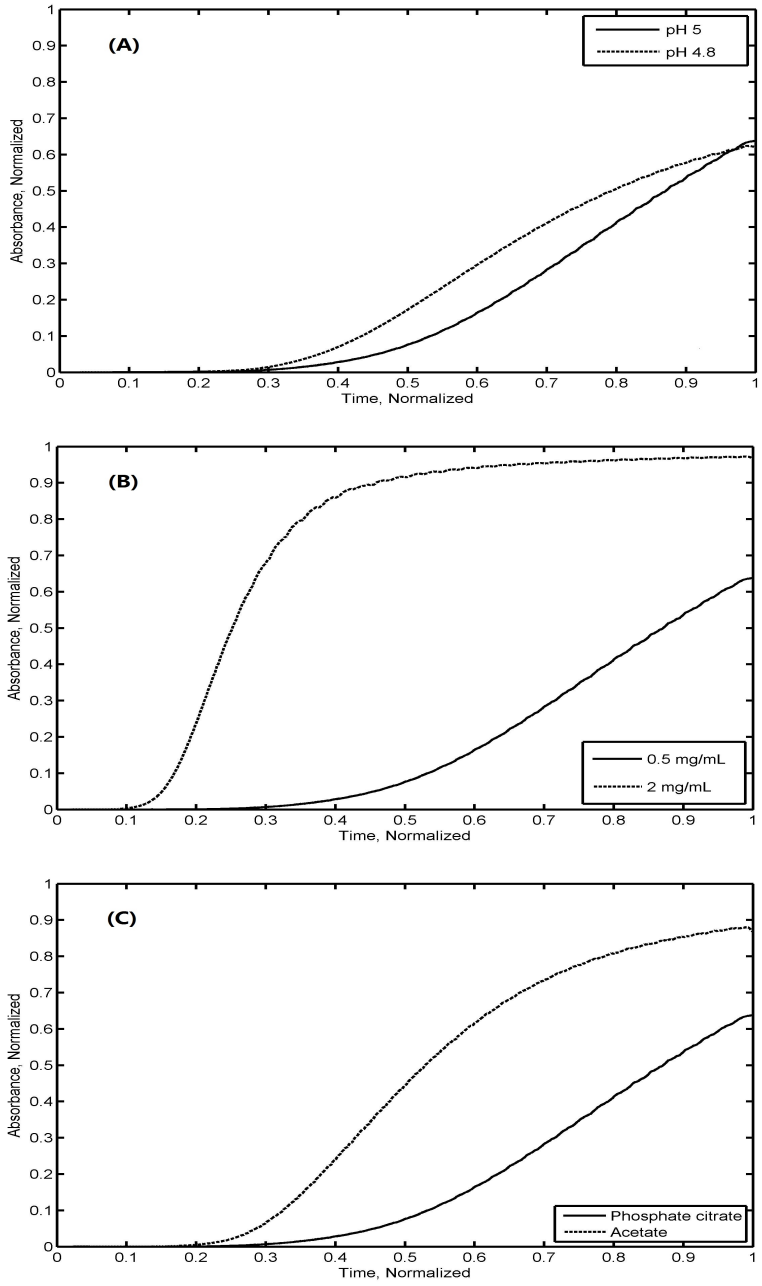

Figure 3-11 Breakthrough curves of lysozyme with Natrix C membrane in various buffer conditions: (A) Comparison of buffer pH; (B) Comparison of feed lysozyme concentration; (C) Comparison of buffer type. Normalized absorbance denotes current absorbance over feed absorbance and normalized time denotes current time over total binding time.

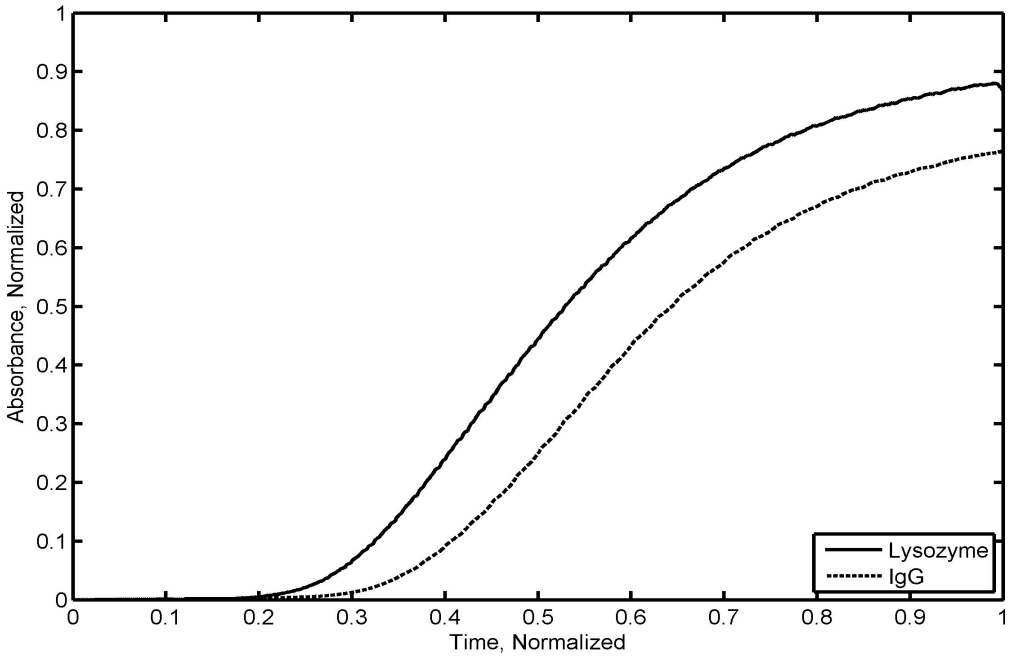

Figure 3-12 Breakthrough curves of lysozyme and IgG with Natrix C membrane in pH 5 acetate buffer with feed protein concentration of 0.5 mg/mL, where normalized absorbance denotes current absorbance over feed absorbance and normalized time denotes current time over total binding time.

The protein binding efficiency according to protein type was obtained from the 10% dynamic binding capacities ($DBC_{10\%}$) of lysozyme and IgG with Natrix C in phosphate citrate buffer and acetate buffer, at different binding condition (Table 3-10). $DBC_{10\%}$ for lysozyme at high protein concentration (2 mg/mL) were smaller than the equilibrium static protein binding estimates, where q_e was 255 ± 10 mg/mL in phosphate citrate buffer and 238 ± 3 mg/mL in acetate buffer (Section 3.3.2.1). This is probably due to an unreached equilibrium state in the flow-through mode. One needs to keep in mind that for conditions at feed protein concentration of 0.5 mg/mL the binding step was incomplete.

The $DBC_{10\%}$ for lysozyme with the Natrix C membrane ranged from 89 mg/mL to 178 mg/mL, comparable to the $DBC_{10\%}$ of lysozyme with poly(acrylic acid) modified regenerated cellulose membrane with 5 mg/mL lysozyme in 10 mM potassium phosphate buffer at pH 7, at a flow rate of 1 mL/min [46] and lysozyme with Fractogel EMD SO_3^- (M) strong cation exchange membrane in a standard binding buffer at pH 5.5 (16.7 mM MES+16.7 mM HEPES+16.7 mM sodium acetate), with 1 mg/mL feed concentration and 0.4 mL/min flow rate [87] (Table 3-11).

Table 3-10 $DBC_{10\%}$ for lysozyme and IgG with Natrix C membrane in phosphate citrate buffer with different binding buffer conditions and feed concentration. (n=3)

Binding buffer type	Binding buffer pH	Feed protein concentration (mg/mL)	DBC $_{10\%}$ (mg/mL)	
			Lysozyme	IgG
Phosphate citrate	4.8	0.5	109 ± 12	-
		2.0	117 ± 41	-
	5	0.5	151 ± 6	-
		2.0	178 ± 8	-
Acetate	5	0.5	89±3	115±7
		2.0	-	-

Table 3-11 Published $DBC_{10\%}$ for lysozyme with cation exchange materials.

Material	pH (binding buffer)	Feed lysozyme concentration (mg/mL)	10% Dynamic binding capacity (mg/mL)	Reference
Sartobind S	7	2	30.4	[71]
	4.5	0.93	13.2	[79]
Sartobind C	-	-	21.8	[46]
Poly (acrylic acid) modified regenerated cellulose membrane (1h modified)	7	5	71.2	[46]
Fractogel EMD SO_3^- (M) (Strong cation)	5.5	1	74	[87]
Fractogel SE HICAP (M) (Strong cation)	5.5	1	51	[87]
Fractogel EMD COO^- (M) (Weak cation)	5.5	1	47	[87]

The pH of a binding buffer had a significant influence on the $DBC_{10\%}$ of lysozyme, evaluated statistically by analysis of variance (ANOVA) with a confidence level of 95%. The $DBC_{10\%}$ increased 39% and 52% from pH 4.8 to pH 5, at feed lysozyme concentration of 0.5mg/mL and 2mg/mL, respectively. The two pH conditions investigated are below the pK_a (5.3) of the membrane, where a positive zeta potential (+ 1 mV) for the membrane (pH 4.8) and a nearly zero zeta potential (pH 5) were observed. [16] With a pI of 11, lysozyme carries strong positive charges in the pH range of 4.5-5. Therefore, the electrostatic interactions are more favorable at pH 5, which may result in the higher binding capacity. Changing the buffer pH may also influence the charge characteristics of protein. Dismer *et al.* [23, 88] proposed that pH of the mobile phase may affect the binding orientation of lysozyme with SP Sepharose FF by changing the surface charge distribution of lysozyme, and confirmed the theory with retention experiments at a pH range of 5-12. Thus it is proposed that the higher binding capacity at pH 5 may result from strong local charged region on the surface of lysozyme.

Other than surface charge characteristics of the membrane and the protein, dynamic protein binding is also determined by membrane morphology. In the previous section (Section 3.3.1.1) on membrane swelling presented significant effect of pH on the membrane swelling, where q_{ms} increased 65% from pH 4.5 to pH 5 in phosphate citrate buffer (0 M). The change of swelling behavior with pH may lead to better availability of binding sites on the membrane.

The feed lysozyme concentration also influenced the dynamic binding capacity. The effect of feed lysozyme concentration was less pronounced than that of buffer pH, as evaluated statistically by analysis of variance (ANOVA) with 95% confidence. The $DBC_{10\%}$ increased 7% and 18% when the feed lysozyme concentration increased from 0.5 mg/mL to 2 mg/mL, at pH 4.8 and 5, respectively. A more significant effect of protein concentration on protein adsorption was observed during static binding, where the equilibrium static binding capacity of lysozyme with Natrix C in pH 5 phosphate citrate buffer with lysozyme concentration of 2 mg/mL (q_e=255 mg/mL) was nearly three times than for 0.5 mg/mL lysozyme concentration (q_e= 85 mg/mL).

The effect of buffer type on dynamic protein binding was investigated for lysozyme and IgG with Natrix C membrane, binding buffer at pH 5 with a feed concentration of 0.5 mg/mL. Buffer type showed a significant effect on lysozyme, where the $DBC_{10\%}$ in phosphate citrate buffer was 70% higher than in acetate buffer. This is different than the static protein binding estimates for lysozyme (Section 3.3.2.1) where similar static binding capacities was observed for the two buffer types over a large concentration range. Since the external mass transport limitations are minimized during the dynamic mode, it is

proposed that the buffer type may have different influence on internal mass transport resistances, leading to differences in $DBC_{10\%}$. When comparing the $DBC_{10\%}$ in the acetate buffer of lysozyme and IgG with the Natrix C membrane, higher $DBC_{10\%}$ was observed for IgG than lysozyme (*i.e.* 23% higher $DBC_{10\%}$).

For IgG, dynamic binding operation with the phosphate citrate buffer could not be completed because of significant pressure increase exceeding the maximum pressure limits. It was postulated that the results were due to a combination of the molecular size of protein and salt-out effect caused by multivalent anions. Hofmeister proposed that salts have different effects on the solubility of proteins and the stability of their secondary and tertiary structure [89]. The salt-out effect of anions is listed as citrate > phosphate > acetate > chloride. With a molecular weight 10 times larger than lysozyme, the aggregation of IgG in phosphate citrate buffer may result in blocking the membrane pores. However, the pore size of Natrix C membrane is up to 100 times larger than the size of IgG and the effluent was transparent without any visible aggregation. In addition, the breakthrough curves (Figure 3-11 C) showed stronger mass transport limitations in phosphate citrate buffer than in acetate buffer. Thus further investigations are needed to understand the effect of phosphate citrate buffer on the dynamic binding of IgG.

The dynamic binding capacity can be significantly influenced by the type and conditions of binding buffer, while protein recovery is determined by the elution buffer. The full chromatograms of lysozyme for two buffer types are given in Figure 3-12, where the first peak denotes the end of binding and the second peak denotes the highest elution point. For phosphate citrate binding buffer at pH 5, the elution buffer was phosphate citrate buffer at pH 7 with 1 M KCl. For acetate binding buffer at pH 5, the elution buffer was phosphate buffer at pH 7 with 1 M KCl. The elution curve showed that elution took place earlier with the phosphate citrate elution buffer, while the peak was higher for the phosphate elution buffer. The recovery could not be calculated due to difficulties in determining the calibration curve for lysozyme, which could be alleviated by collecting the fractions after the elution step and measuring their lysozyme content. The effect of conditions of elution buffer on dynamic protein capture would also be of great interest for further investigation.

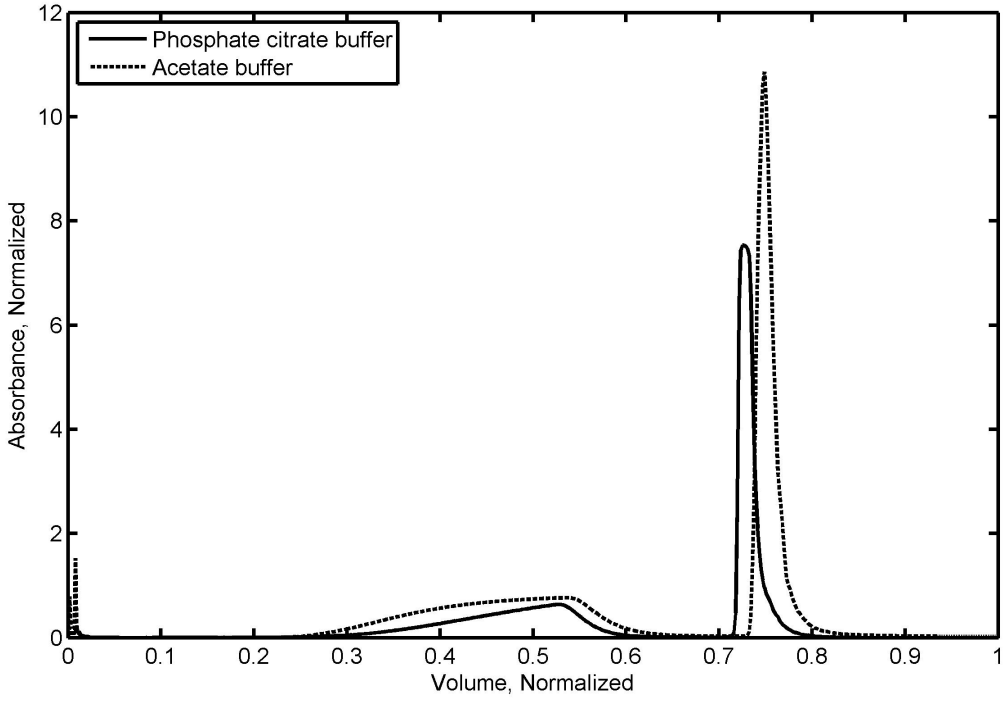

Figure 3-13 Full chromatogram of lysozyme with Natrix C membrane. Binding buffer was phosphate citrate buffer and acetate buffer, at pH 5 with feed lysozyme concentration of 0.5 mg/mL, where normalized absorbance denotes current absorbance over feed absorbance and normalized volume denotes current volume over total volume.

Chapter 4
Conclusions

The present work was to investigate the effect of buffer on the membrane properties and protein capture with a weak cation exchange macroporous hydrogel membrane, Natrix C. The first objective focused on the effect of buffer on membrane properties, namely the membrane swelling behavior and its surface morphology observed by Environmental Scanning Electron Microscopy (ESEM). Two types of buffer with different ion characteristics, phosphate citrate buffer and acetate buffer, were compared. The swelling experiments confirmed that pH had a significant influence (ANOVA; 95%) on membrane swelling for phosphate citrate and acetate buffer through electrostatic repulsions. At constant ionic strength, the swelling factor increased significantly with pH at first and then leveled off after pH 6.0, where the pores of hydrogel almost reached its maximum size. The effect of ionic strength on membrane swelling was less significant (ANOVA; 95%), and was dependent on pH. The decreasing swelling factor with ionic strength mainly resulted from osmosis and electrostatic repulsions. The swelling factors between the two types of buffer were not significantly different (paired t-test; 95%). Surface pore structure visualized by ESEM of Natrix C membrane, dried and buffer equilibrated with subsequent freeze-drying indicated significant effect of the hydrogel component.

The second objective was to investigate the effect of buffer on static protein adsorption by comparing two different proteins, lysozyme and IgG, through protein adsorption isotherms. The two parameters of the Langmuir model, which is based on monolayer coverage and independent binding sites, indicated different maximum adsorption capacity (q_{max}) and protein membrane affinity (K) according to protein type and buffer conditions. For lysozyme, the estimated q_{max} was similar for the phosphate citrate and acetate buffer while the estimated K was five times larger in phosphate citrate buffer than for acetate buffer. For IgG, the two estimated Langmuir parameters were significantly different between the two buffers. The difference in the estimated K value between phosphate citrate buffer and acetate buffer may result from the effect of ion composition of buffer on surface charge distribution of protein surface or hydrophobic interactions between the protein and the membrane, while the differences in estimated q_{max} may reflect the effect of ionic strength of buffer. The estimated Langmuir parameters between lysozyme and IgG were mainly dependent on the protein size and number of basic (acidic) surface residues. With smaller size and stronger positive charges, lysozyme achieved higher static binding capacity and stronger adsorption affinity than IgG. Therefore the protein charge dominated while the buffer effect on adsorption

isotherm was negligible for lysozyme. For IgG, the protein charge was moderate while the buffer effect was significant.

The significant influence of salt counter-ion concentration (ionic strength) on static protein binding of IgG was confirmed by investigating the effect of ion content on the estimated Langmuir parameters for IgG with Natrix C membrane in phosphate citrate buffer and acetate buffer. The estimated q_{max} decreased linearly with ionic strength, probably due to reduced accessibility of binding sites and competitive binding between salt and protein. The estimated K increased with ionic strength, which contradicted with trends observed in the literature for lysozyme and may be explained by the complex surface characteristics of IgG and distinct microstructure of Natrix C membrane.

The ability to characterize protein membrane interactions was investigated with the SMA adsorption model and IgG adsorption isotherms. The characteristic charge (ν), indicating the number of charged sites on the protein that interacts with the membrane, was determined as 4.52 in phosphate citrate buffer and 2.08 in acetate buffer, respectively. This may be due to the adsorption of multivalent anions in phosphate citrate buffer onto the protein surface that affect the surface charge distribution. The equilibrium constant (K_a) was estimated to be 18% higher in phosphate citrate buffer than in acetate buffer, in agreement with estimated Langmuir parameters, where higher estimated K was also obtained for phosphate citrate buffer. The steric factor (σ), which denotes the number of sites on the membrane surface that are shielded by the adsorbed, in phosphate citrate buffer was half the one estimated for acetate buffer. These differences may reflect the influence of ion content on the binding orientation and/or conformational changes of IgG that lead to smaller contact area with the membrane surface. SMA model parameters sensitivity analysis revealed that all above three parameters influenced the SMA model protein adsorption estimates, with ν the most significant while σ the least.

The third objective was to evaluate the effect of buffer on dynamic protein adsorption, *i.e.* feed protein concentration, pH and type of binding buffer by analyzing the breakthrough curves and dynamic binding capacity estimates at 10% breakthrough ($DBC_{10\%}$). Dynamic binding of IgG was strongly dependent on buffer type. Higher $DBC_{10\%}$ than lysozyme was achieved in acetate buffer, while the dynamic binding operation was inaccessible with the phosphate citrate buffer.

Distinct breakthrough curves were obtained for lysozyme at different pH, feed concentration and buffer type. Earlier breakthrough and/or steeper slope were observed at conditions with pH 4.8, 2 mg/mL feed lysozyme concentration, and acetate buffer, respectively, indicating less mass transport limitations. The estimated $DBC_{10\%}$ for lysozyme were lower than its corresponding equilibrium static binding capacity at

high protein concentration, probably due to unreached equilibrium state in the flow-through mode. Significant effect of pH and moderate effect of feed concentration on $DBC_{10\%}$ were observed for lysozyme with Natrix C membrane (ANOVA; 95%). It was proposed that buffer pH affected dynamic protein binding by influencing surface charge characteristics of membrane and protein, as well as membrane swelling, which may affect the availability of binding sites on the membrane. The effect of buffer type on $DBC_{10\%}$ was found to be significant for lysozyme (ANOVA; 95%). However, this difference was not observed for the static binding capacity of lysozyme.

With the higher static and dynamic binding capacity obtained in this study, Natrix C membranes are proposed to be a promising alternative to other commercial cation exchange resins and membranes for protein capture. Further investigations on the mass transport and flow distribution of membrane modules will be needed to scale up for industrial use.

Chapter 5
Recommendations

Based on the results obtained in this thesis, the following recommendations are proposed for future investigations on protein capture with cation exchange membrane chromatography.

(1) Quantitative characterization of the pore structure for ion exchange membranes

Due to difficulties in properly defining pore contours with the current image analysis system, the pore size and pore size distribution could not be quantitatively characterized. The ESEM images revealed a complex pore structure that would require the development or use of a combination of characterization methods for pore structure such as reported in [58].

(2) Protein labeling

Significant effect of buffer type on protein static/dynamic binding was observed in the present work and its influence on binding orientation was proposed. Further investigations on this point will be needed and could be achieved by labeling of lysine residue of the protein and using fluorescence imaging [22].

(3) Mass transfer analysis for dynamic protein binding

The breakthrough curves obtained in the present work showed various shape and slope according to buffer conditions, rather than the rectangular shape for ideal adsorbents. It indicated the existence of mass transport limitations during dynamic binding with Natrix C membrane, which requires further investigations. Numerous mathematical models [84-86] accounting for the mass transport resistances during dynamic binding of protein with ion exchange membranes should be investigated to narrow in onto a better explanation of the observed effects.

(4) Optimization of elution conditions

The present work investigated the effect of binding buffer on dynamic protein binding and observed significant effect of buffer pH and buffer type. Further investigations should be made on conditions of elution buffer, *i.e.* pH, type, and flow rate.

References

[1] U. Gottschalk, Bioseparation in Antibody Manufacturing: The Good, The Bad and The Ugly, Biotechnology Progress, 24 (2008) 496-503.
[2] N.S. Inc., Natrix HD-C Hydrogel Membrane Weak Cation Exchange Chromatography, in: N.S. Inc. (Ed.), Canada.
[3] G. Healthcare, Ion Exchange Chromatography & Chromatofocusing-Principles and Methods, in: G. Healthcare (Ed.), 2010.
[4] D. Low, R. O'Leary, N.S. Pujar, Future of antibody purification, Journal of Chromatography B, 848 (2007) 48-63.
[5] S. Hober, K. Nord, M. Linhult, Protein A chromatography for antibody purification, Journal of Chromatography B, 848 (2007) 40-47.
[6] R. Boyer, Modern Experimental Biochemistry, Addison Wesley Longman, 2000.
[7] L. Zhong, J. Scharer, M. Moo-Young, D. Fenner, L. Crossley, C.H. Honeyman, S.-Y. Suen, C.P. Chou, Potential application of hydrogel-based strong anion-exchange membrane for plasmid DNA purification, Journal of Chromatography B, 879 (2011) 564-572.
[8] R. Ghosh, Protein separation using membrane chromatography: opportunities and challenges, Journal of Chromatography A, 952 (2002) 13-27.
[9] V. Orr, L. Zhong, M. Moo-Young, C.P. Chou, Recent advances in bioprocessing application of membrane chromatography, Biotechnology Advances, 31 (2013) 450-465.
[10] T. Hashimoto, Non-porous hydrophilic resin-based packings for the separation of biopolymers, Journal of Chromatography A, 544 (1991) 257-265.
[11] C. Boi, Membrane adsorbers as purification tools for monoclonal antibody purification, Journal of Chromatography B, 848 (2007) 19-27.
[12] S.-Y. Suen, M.R. Etzel, A mathematical analysis of affinity membrane bioseparations, Chemical Engineering Science, 47 (1992) 1355-1364.
[13] C.-S. Chang, S.-Y. Suen, Modification of porous alumina membranes with n-alkanoic acids and their application in protein adsorption, Journal of Membrane Science, 275 (2006) 70-81.
[14] N.S. Inc., Lab Scale Product Catalogue, in: N.S. Inc. (Ed.), Burlington.
[15] A.W. Chan, R.J. Neufeld, Modeling the controllable pH-responsive swelling and pore size of networked alginate based biomaterials, Biomaterials, 30 (2009) 6119-6129.
[16] A.-K.J. Hassel, Protein Capture by Cation Exchange Membranes, in: Chemical Engineering, University of Waterloo, 2015.
[17] K. Liburdi, I. Benucci, M. Esti, Lysozyme in Wine: An Overview of Current and Future Applications, Comprehensive Reviews in Food Science and Food Safety, 13 (2014) 1062-1073.
[18] B.M. Chassy, A. Giuffrida, Method for the lysis of Gram-positive, asporogenous bacteria with lysozyme, Applied and environmental microbiology, 39 (1980) 153-158.
[19] V. Calandrini, D. Fioretto, G. Onori, A. Santucci, Role of hydrophobic interactions on the stabilisation of native state of globular proteins, Chemical Physics Letters, 324 (2000) 344-348.
[20] S. Chattoraj, A.K. Mandal, K. Bhattacharyya, Effect of ethanol-water mixture on the structure and dynamics of lysozyme: A fluorescence correlation spectroscopy study, The Journal of Chemical Physics, 140 (2014) 115105.
[21] W.S. Price, F. Tsuchiya, Y. Arata, Time Dependence of Aggregation in Crystallizing Lysozyme Solutions Probed Using NMR Self-Diffusion Measurements, Biophysical Journal, 80 (2001) 1585-1590.
[22] F. Dismer, J. Hubbuch, A novel approach to characterize the binding orientation of lysozyme on ion-exchange resins, Journal of Chromatography A, 1149 (2007) 312-320.

[23] F. Dismer, M. Petzold, J. Hubbuch, Effects of ionic strength and mobile phase pH on the binding orientation of lysozyme on different ion-exchange adsorbents, Journal of Chromatography A, 1194 (2008) 11-21.
[24] J. Koolman, K.-H. Röhm, Color atlas of biochemistry, Thieme, 2005.
[25] B.M. Tande, N.J. Wagner, M.E. Mackay, C.J. Hawker, M. Jeong, Viscosimetric, hydrodynamic, and conformational properties of dendrimers and dendrons, Macromolecules, 34 (2001) 8580-8585.
[26] V. Ball, A. Bentaleb, J. Hemmerle, J.-C. Voegel, P. Schaaf, Dynamic aspects of protein adsorption onto titanium surfaces: mechanism of desorption into buffer and release in the presence of proteins in the bulk, Langmuir, 12 (1996) 1614-1621.
[27] M.T. Tyn, T.W. Gusek, Prediction of diffusion coefficients of proteins, Biotechnology and bioengineering, 35 (1990) 327-338.
[28] U. Rutishauser, B.A. Cunningham, C. Bennett, W.H. Konigsberg, G.M. Edelman, Amino acid sequence of the Fc region of a human gamma G-immunoglobulin, Proceedings of the National Academy of Sciences of the United States of America, 61 (1968) 1414.
[29] T. Paterson, J. Innes, L. McMillan, I. Downing, M.C.M. Carter, Variation in IgG1 heavy chain allotype does not contribute to differences in biological activity of two human anti-Rhesus (D) monoclonal antibodies, Immunotechnology, 4 (1998) 37-47.
[30] P.R. Baum, E.S. Espling, P. Tan, P.A. Thompson, Binding proteins comprising immunoglobulin hinge and fc regions having altered fc effector functions, in, Google Patents, 2007.
[31] D. Yu, R. Ghosh, Enzymatic fragmentation of cation exchange membrane bound immunoglobulin G, Biotechnology progress, 27 (2011) 61-66.
[32] N. Forrer, A. Butté, M. Morbidelli, Chromatographic behavior of a polyclonal antibody mixture on a strong cation exchanger column. Part I: Adsorption characterization, Journal of Chromatography A, 1214 (2008) 59-70.
[33] K. Wrzosek, M. Polakovič, Effect of pH on protein adsorption capacity of strong cation exchangers with grafted layer, Journal of Chromatography A, 1218 (2011) 6987-6994.
[34] T. Gura, Therapeutic antibodies: magic bullets hit the target, Nature, 417 (2002) 584-586.
[35] D.R. Lide, CRC Handbook of Chemistry and Physics, 83rd ed., CRC Press, 2002.
[36] E. Komkova, Principles of Ion-Exchange Chromatography for Buffer Optimization, in, Natrix Separations Inc. , Burlington, 2010.
[37] D.B. Burns, A.L. Zydney, Buffer effects on the zeta potential of ultrafiltration membranes, Journal of Membrane Science, 172 (2000) 39-48.
[38] A. Faude, D. Zacher, E. Müller, H. Böttinger, Fast determination of conditions for maximum dynamic capacity in cation-exchange chromatography of human monoclonal antibodies, Journal of Chromatography A, 1161 (2007) 29-35.
[39] C. Harinarayan, J. Mueller, A. Ljunglöf, R. Fahrner, J. Van Alstine, R. Van Reis, An exclusion mechanism in ion exchange chromatography, Biotechnology and bioengineering, 95 (2006) 775-787.
[40] D. Karlsson, N. Jakobsson, K.-J. Brink, A. Axelsson, B. Nilsson, Methodologies for model calibration to assist the design of a preparative ion-exchange step for antibody purification, Journal of Chromatography A, 1033 (2004) 71-82.
[41] G. Limousin, J.-P. Gaudet, L. Charlet, S. Szenknect, V. Barthes, M. Krimissa, Sorption isotherms: a review on physical bases, modeling and measurement, Applied Geochemistry, 22 (2007) 249-275.
[42] M.C. Ncibi, Applicability of some statistical tools to predict optimum adsorption isotherm after linear and non-linear regression analysis, Journal of Hazardous Materials, 153 (2008) 207-212.
[43] K. Vijayaraghavan, T. Padmesh, K. Palanivelu, M. Velan, Biosorption of nickel (II) ions onto Sargassum wightii: application of two-parameter and three-parameter isotherm models, Journal of Hazardous Materials, 133 (2006) 304-308.

[44] G.L. Skidmore, B.J. Hortsmann, H.A. Chase, Modelling single-component protein adsorption to the cation exchanger s sepharose® FF, Journal of Chromatography A, 498 (1990) 113-128.
[45] Y. Wei, J. Ma, C. Wang, Preparation of high-capacity strong cation exchange membrane for protein adsorption via surface-initiated atom transfer radical polymerization, Journal of Membrane Science, 427 (2013) 197-206.
[46] N. Singh, J. Wang, M. Ulbricht, S.R. Wickramasinghe, S.M. Husson, Surface-initiated atom transfer radical polymerization: a new method for preparation of polymeric membrane adsorbers, Journal of Membrane Science, 309 (2008) 64-72.
[47] H. Yang, M.R. Etzel, Evaluation of three kinetic equations in models of protein purification using ion-exchange membranes, Industrial & engineering chemistry research, 42 (2003) 890-896.
[48] W. Kopaciewicz, M.A. Rounds, J. Fausnaugh, F.E. Regnier, Retention model for high-performance ion-exchange chromatography, Journal of Chromatography A, 266 (1983) 3-21.
[49] C.A. Brooks, S.M. Cramer, Steric mass-action ion exchange: Displacement profiles and induced salt gradients, AIChE Journal, 38 (1992) 1969-1978.
[50] R. Drager, F. Regnier, Application of the stoichiometric displacement model of retention to anion-exchange chromatography of nucleic acids, Journal of Chromatography A, 359 (1986) 147-155.
[51] M.A. Rounds, F.E. Regnier, Evaluation of a retention model for high-performance ion-exchange chromatography using two different displacing salts, Journal of Chromatography A, 283 (1984) 37-45.
[52] V. A, Studies in Nonlinear Chromatography, in, Yale University, 1990.
[53] S.R. Gallant, A. Kundu, S.M. Cramer, Optimization of step gradient separations: Consideration of nonlinear adsorption, Biotechnology and bioengineering, 47 (1995) 355-372.
[54] A. Ladiwala, K. Rege, C.M. Breneman, S.M. Cramer, A priori prediction of adsorption isotherm parameters and chromatographic behavior in ion-exchange systems, Proceedings of the National Academy of Sciences of the United States of America, 102 (2005) 11710-11715.
[55] H. Shen, D.D. Frey, Effect of charge regulation on steric mass-action equilibrium for the ion-exchange adsorption of proteins, Journal of Chromatography A, 1079 (2005) 92-104.
[56] W.-D. Chen, H.-H. Hu, Y.-D. Wang, Analysis of steric mass-action model for protein adsorption equilibrium onto porous anion-exchange adsorbent, Chemical engineering science, 61 (2006) 7068-7076.
[57] A. Osberghaus, S. Hepbildikler, S. Nath, M. Haindl, E. von Lieres, J. Hubbuch, Determination of parameters for the steric mass action model—A comparison between two approaches, Journal of Chromatography A, 1233 (2012) 54-65.
[58] P. DePhillips, A.M. Lenhoff, Determinants of protein retention characteristics on cation-exchange adsorbents, Journal of Chromatography A, 933 (2001) 57-72.
[59] K. Wrzosek, M. Gramblička, M. Polakovič, Influence of ligand density on antibody binding capacity of cation-exchange adsorbents, Journal of Chromatography A, 1216 (2009) 5039-5044.
[60] H.-L. Lu, D.-Q. Lin, M.-M. Zhu, S.-J. Yao, Effects of ligand density and pore size on the adsorption of bovine IgG with DEAE ion-exchange resins, Journal of Separation Science, 35 (2012) 2131-2137.
[61] I. Tatárová, R. Fáber, R. Denoyel, M. Polakovič, Characterization of pore structure of a strong anion-exchange membrane adsorbent under different buffer and salt concentration conditions, Journal of Chromatography A, 1216 (2009) 941-947.
[62] J. Wang, F. Dismer, J. Hubbuch, M. Ulbricht, Detailed analysis of membrane adsorber pore structure and protein binding by advanced microscopy, Journal of Membrane Science, 320 (2008) 456-467.

[63] T.M. Pabst, G. Carta, pH transitions in cation exchange chromatographic columns containing weak acid groups, Journal of Chromatography A, 1142 (2007) 19-31.
[64] Q. Shi, Y. Zhou, Y. Sun, Influence of pH and Ionic Strength on the Steric Mass‐Action Model Parameters around the Isoelectric Point of Protein, Biotechnology progress, 21 (2005) 516-523.
[65] D.C. Montgomery, D.C. Montgomery, D.C. Montgomery, Design and analysis of experiments, Wiley New York, 1984.
[66] S. Yarimkaya, H. Basan, Swelling behavior of poly (2‐hydroxyethyl methacrylate‐co‐acrylic acid‐co‐ammonium acrylate) hydrogels, Journal of Macromolecular Science, Part A: Pure and Applied Chemistry, 44 (2007) 939-946.
[67] T. Sata, Ion exchange membranes: preparation, characterization, modification and application, Royal Society of chemistry, 2004.
[68] S.J. Kim, S.R. Shin, D.I. Shin, I.Y. Kim, S.I. Kim, Synthesis and characteristics of semi‐interpenetrating polymer network hydrogels based on chitosan and poly (hydroxy ethyl methacrylate), Journal of applied polymer science, 96 (2005) 86-92.
[69] V.M. Barragán, J.P.G. Villaluenga, M.P. Godino, M.A. Izquierdo-Gil, C. Ruiz-Bauzá, B. Seoane, Swelling and electro-osmotic properties of cation-exchange membranes with different structures in methanol–water media, Journal of Power Sources, 185 (2008) 822-827.
[70] A. Osberghaus, P. Baumann, S. Hepbildikler, S. Nath, M. Haindl, E. von Lieres, J. Hubbuch, Detection, Quantification, and Propagation of Uncertainty in High‐Throughput Experimentation by Monte Carlo Methods, Chemical engineering & technology, 35 (2012) 1456-1464.
[71] I. Tatárová, P. Dreveňák, A. Kosior, M. Polakovič, Equilibrium and kinetics of protein binding on ion-exchange cellulose membranes with grafted polymer layer, Chem. Pap., 67 (2013) 1527-1536.
[72] S.-Y. Lin, S.-Y. Suen, Protein separation using plate-and-frame modules with ion-exchange membranes, Journal of Membrane Science, 204 (2002) 37-51.
[73] F.-Y. Lin, W.-Y. Chen, Microcalorimetric Studies on the Interaction Mechanism between Proteins and Hydrophobic Solid Surfaces in Hydrophobic Interaction Chromatography: Effects of Salts, Hydrophobicity of the Sorbent, and Structure of the Protein, Analytical Chemistry, 73 (2001) 3875-3883.
[74] M.T. Hearn, Physicochemical factors in polypeptide and protein purification and analysis by high-performance liquid chromatographic techniques: current status and challenges for the future, Separation Science and Technology, 2 (2000) 71-235.
[75] H. Ikeda, A. Suzuki, Wettability Effects of Plate Materials on Hydrodynamics in a Pulsed Perforated-Plate Extraction Column of Pulser Feeder Type, Industrial & Engineering Chemistry Research, 34 (1995) 4110-4117.
[76] T. Müller-Späth, G. Ströhlein, L. Aumann, H. Kornmann, P. Valax, L. Delegrange, E. Charbaut, G. Baer, A. Lamproye, M. Jöhnck, Model simulation and experimental verification of a cation-exchange IgG capture step in batch and continuous chromatography, Journal of Chromatography A, 1218 (2011) 5195-5204.
[77] K. Wrzosek, P. Ačai, M. Gramblička, M. Polakovič, Modeling of equilibrium and kinetics of human polyclonal immunoglobulin G adsorption on a tentacle cation exchanger, Chem. Pap., 67 (2013) 1537-1547.
[78] S. Wickramasinghe, J. Carlson, C. Teske, J. Hubbuch, M. Ulbricht, Characterizing solute binding to macroporous ion exchange membrane adsorbers using confocal laser scanning microscopy, Journal of membrane science, 281 (2006) 609-618.
[79] P. van Beijeren, P. Kreis, T. Zeiner, Ion exchange membrane adsorption of bovine serum albumin—Impact of operating and buffer conditions on breakthrough curves, Journal of Membrane Science, 415 (2012) 568-576.

[80] E. Dzhafarov, [Conformational transitions of human serum albumin depending on pH. Study using tritium markers], Molekuliarnaia biologiia, 25 (1990) 1412-1417.
[81] S.D. Gadam, G. Jayaraman, S.M. Cramer, Characterization of non-linear adsorption properties of dextran-based polyelectrolyte displacers in ion-exchange systems, Journal of Chromatography A, 630 (1993) 37-52.
[82] S.R. Gallant, S.M. Cramer, Productivity and operating regimes in protein chromatography using low-molecular-mass displacers, Journal of Chromatography A, 771 (1997) 9-22.
[83] K. Gebauer, J. Thömmes, M. Kula, Breakthrough performance of high-capacity membrane adsorbers in protein chromatography, Chemical engineering science, 52 (1997) 405-419.
[84] P. Francis, E. von Lieres, C. Haynes, Zonal rate model for stacked membrane chromatography part II: Characterizing ion‐exchange membrane chromatography under protein retention conditions, Biotechnology and bioengineering, 109 (2012) 615-629.
[85] F.T. Sarfert, M.R. Etzel, Mass transfer limitations in protein separations using ion-exchange membranes, Journal of chromatography A, 764 (1997) 3-20.
[86] H. Yang, M. Bitzer, M.R. Etzel, Analysis of protein purification using ion-exchange membranes, Industrial & engineering chemistry research, 38 (1999) 4044-4050.
[87] A. Staby, J.H. Jacobsen, R.G. Hansen, U.K. Bruus, I.H. Jensen, Comparison of chromatographic ion-exchange resins: V. Strong and weak cation-exchange resins, Journal of chromatography A, 1118 (2006) 168-179.
[88] F. Dismer, J. Hubbuch, 3D structure-based protein retention prediction for ion-exchange chromatography, Journal of Chromatography A, 1217 (2010) 1343-1353.
[89] R.L. Baldwin, How Hofmeister ion interactions affect protein stability, Biophysical journal, 71 (1996) 2056.